

Contents lists available at [ScienceDirect](https://www.sciencedirect.com)

## European Journal of Mechanics / A Solids

journal homepage: [www.elsevier.com/locate/ejmsol](http://www.elsevier.com/locate/ejmsol)

# Nonlinear thermal dynamic buckling and global optimization of smart sandwich plate with porous homogeneous core and carbon nanotube reinforced nanocomposite layers

Ngo Dinh Dat<sup>a</sup>, Tran Quoc Quan<sup>a,b,\*</sup>, Nguyen Dinh Duc<sup>c</sup>

<sup>a</sup> Phenikaa Institute for Advanced Study (PIAS), Phenikaa University, Hanoi, 12116, Viet Nam

<sup>b</sup> Faculty of Mechanical Engineering and Mechatronics, Phenikaa University, Hanoi, 12116, Viet Nam

<sup>c</sup> Department of Engineering and Technology in Constructions and Transportation – VNU Hanoi, University of Engineering and Technology, 144 – Xuan Thuy, Cau Giay, Hanoi, Viet Nam

## ARTICLE INFO

## Keywords:

Nonlinear thermal dynamic buckling  
Global optimization  
Smart sandwich plate  
Carbon nanotube reinforced nanocomposite  
Bees algorithm

## ABSTRACT

The analytical investigation for the nonlinear thermal dynamic buckling of smart sandwich plate subjected to mechanical, thermal and electric loadings is presented. The sandwich plate is composed of a porous homogeneous core, two carbon nanotube reinforced composite (CNTRC) layers and two piezoelectric face sheets. Basic equations are derived based on the Reddy's higher order shear deformation plate theory and Hamilton's principle in which the initial imperfection and Pasternak-type elastic foundations are included. The external pressure is assumed to be uniformly distributed on the surface of the sandwich plate and depend on time according to the linear functions. The nonlinear dynamic response, the frequency – amplitude relation are obtained by using the Galerkin and Runge – Kutta methods and the critical dynamic buckling load is determined by using Budiansky – Roth criterion. Bees Algorithm is used to determine the maximum value of natural frequency of smart sandwich plate and the corresponding optimum values of geometrical and material parameters. The effects of geometrical parameters, CNT volume fraction, elastic foundations, temperature increment, initial imperfection and porosity coefficient on the nonlinear vibration and dynamic buckling of the smart sandwich plate are considered specifically. The numerical results are also compared with existing results using different theories.

## 1. Introduction

Porous materials are promising class of solid materials containing pores or voids. The material properties of porous materials depend on the shape, size and volume fraction of the pores. The porosity increases the surface area of materials, which improves the interaction of the material with the external impacts. In recent decades, porous materials are used in a wide range of applications such as catalyst supports, chemical separations, gas sensors and adsorption. Therefore, the design, synthesis and behaviors of porous materials have attracted the great attention of engineers and materials scientists. [Saidi et al. \(2019\)](#) investigated the vibration and stability analyses of functionally graded reinforced porous plates with piezoelectric layers under supersonic flow based on the first order shear deformation plate theory and first order piston theory. [Ansari et al. \(2020\)](#) introduced an efficient numerical strategy to study the geometrically nonlinear static bending of

functionally graded graphene platelet reinforced composite porous plates with arbitrary shape. [Chen et al. \(2018\)](#) proposed the least square spectral collocation method to predict temperature distribution and heat transfer efficiency of moving porous plate in which two types of boundary conditions are taken into account. [Xie et al. \(2020\)](#) presented a novel approach, based on energy balance method, to deal with the large amplitude nonlinear free vibration problem of the rectangular porous functionally graded plates. Numerical results in this publication illustrate that the nonlinear to linear frequency ratio is less sensitive to the porosity volume fraction than the linear frequency for the porous functionally graded plates. [Xue et al. \(2019\)](#) studied the free vibration of porous square plate, circular plate, and rectangle plate with a central circular hole in the framework of isogeometric analysis using the first order shear deformation theory and the exact geometric models. [Moradi-Dastjerdi et al. \(2020\)](#) presented the buckling resistance of a novel active multidisciplinary sandwich plate which includes an advanced

\* Corresponding author. Phenikaa Institute for Advanced Study (PIAS), Phenikaa University, Hanoi, 12116, Viet Nam.

E-mail address: [quan.tranquoc@phenikaa-uni.edu.vn](mailto:quan.tranquoc@phenikaa-uni.edu.vn) (T.Q. Quan).

<https://doi.org/10.1016/j.euromechsol.2021.104351>

Received 10 March 2021; Received in revised form 22 May 2021; Accepted 17 June 2021

Available online 21 June 2021

0997-7538/© 2021 Elsevier Masson SAS. All rights reserved.

porous core reinforced with carbon nanotubes integrated between two active piezoelectric faces under in-plane mechanical load or temperature change. Further, [Trinh et al. \(2020\)](#) introduced a semi-analytical approach integrated with Monte Carlo simulation for stochastic buckling analyses of porous functionally graded plates arising due to the inevitable source-uncertainties of geometrical configurations and material properties. Based on the third order shear deformation and physical neutral plane theories, thermal postbuckling analysis for functionally graded porous beam are performed in the work of [Babaei et al. \(2020\)](#). [Chen et al. \(2019\)](#) proposed a novel functionally graded porous plate where the continuous gradient in material properties based on a graded porosity offers a smooth stress distribution along the plate thickness so that the remarkable stress mismatch that leads to interfacial failure in the conventional sandwich structures can be avoided.

A single-walled carbon nanotube is a cylinder of carbon atoms with geometrical parameters of less than 1 nm. Because of unique properties such as ideal strength, light weight, high thermal and electrical conductivity, single-walled carbon nanotubes are often chosen to be reinforcement in polymer matrix composite to enhance the material properties of structures. There have been an increasing number of studies on the mechanical behaviors of carbon nanotube reinforced composites (CNTRC) in recent years. [Sofiyev et al. \(2019, 2020\)](#) presented analytical solutions for the vibration and stability of heterogeneous carbon nanotube reinforced composite truncated conical shells under axial load and the stability problem of functionally graded carbon nanotube reinforced composite conical shells exposed to external lateral and hydrostatic pressures based on the first order shear deformation theory and Galerkin method. [Zhang et al. \(2020\)](#) introduced a solution method for studying the static free vibration behaviors of pretwisted hybrid composite blade containing carbon nanotube reinforced composite layers as well as matrix cracked fiber reinforced composite layers; [Qin et al. \(2020\)](#) presented a unified Fourier series solution to solve the vibration problem of functionally graded carbon nanotube-reinforcement composite cylindrical shells, conical shells and annular plates subjected to general boundary conditions. Besides, [Zhu et al. \(2012\)](#) carried out the bending and free vibration analyses of thin-to-moderately thick composite plates reinforced by single-walled carbon nanotubes using the finite element method based on the first order shear deformation plate theory. [Fu et al. \(2019\)](#) presented an accurate and analytical method for investigation the dynamic instability of laminated FG-CNTRC conical shell surrounded by the elastic foundations based on the first-order shear deformation theory. [Shen et al. \(2017a; 2017b, 2013, 2014\)](#) investigated the behaviors of large amplitude vibration, nonlinear bending and thermal postbuckling of nanocomposite beams, cylindrical panels, plates and cylindrical shells reinforced by single-walled carbon nanotubes resting on an elastic foundation in thermal environments using higher order shear deformation plate theory and von Kármán nonlinear strain-displacement relationships. The numerical results show the effects of CNT volume fraction, geometrical parameters and foundation stiffness on the mechanical behaviors of the structures. [Yang et al. \(2020\)](#) reported a study on the large amplitude nonlinear vibration of carbon nanotube-reinforced composite laminated plates with negative Poisson's ratios in thermal environments. Further, [Duc et al. \(2019\)](#) proposed analytical solutions for the nonlinear vibration of imperfect functionally graded nanocomposite double curved shallow shells on elastic foundations subjected to mechanical load in thermal environments.

Due to the ability to flexibly and actively change the mechanical, thermal, electrical, and magnetic properties under the action of external stimulus, smart materials play an important role in creating devices or structures in aerospace, civil engineering, memory capabilities, actuators, sensors and so on. [Karimiasl et al. \(2019\)](#) focused on the nonlinear vibration analysis of composite sandwich doubly curved shell with a flexible core integrated with a piezoelectric layer by using the higher order shear deformable theory and the third-order polynomial theory.

[Mahmoodi et al. \(2020\)](#) presented the bending analysis of laminated carbon nanotube piezo-nanocomposite moderately thick rectangular plates by a multi-scale approach; [Giannopoulos et al. \(2007\)](#) carried out an integrated approach for the buckling behavior of smart beams and plates under multiple loading conditions using discrete layer kinematics. Further, [Sahoo and Ray \(2019\)](#) analyzed the performance of elliptical smart constrained layer damping treatments on active damping of geometrical nonlinear vibrations of smart laminated composite plates. Based on theory of piezoelectricity and using generalized coupled thermoelasticity, [Alibeigloo \(2019\)](#) studied transient response of a simply supported functionally graded material rectangular plate embedded in sensor and actuator piezoelectric layers under applied electric field and thermal shock. [Zoric et al. \(2019\)](#) dealt with optimization of the sizing, location and orientation of the piezo-fiber reinforced composite actuators and active vibration control of the smart composite plates using particle-swarm optimized self-tuning fuzzy logic controller. [Dat et al. \(2020\)](#) investigated the nonlinear magneto-electro-elastic vibration of smart sandwich plate which consists of a carbon nanotube reinforced nanocomposite core integrated with two magneto-electro-elastic face sheets using Reddy's higher order shear deformation theory. An analysis of delaminated composite plates with integrated active fibre composite actuators and sensor under hygro-thermal environment has been undertaken in the work of [Shankar et al. \(2017\)](#) in which hygrothermal loading is taken into consideration, and the effect of moisture and temperature on the delaminated plate structures is analyzed. [Sreehari et al. \(2016\)](#) developed a finite element formulation based on inverse hyperbolic shear deformation theory for handling bending and buckling analysis of a smart composite plates using Hamilton's variational principle. [Farsangi et al. \(2013\)](#) introduced an analytical solution for free vibrations of a hybrid rectangular plate composed of a transversely isotropic, homogeneous and linear elastic core and face sheets made of a linear piezoelectric material by assuming that the plate deformations are governed by the Mindlin plate theory. It is found in this paper that the electric boundary conditions on major surfaces of the piezoelectric layers and the aspect ratio of the hybrid plate noticeably influence its frequencies.

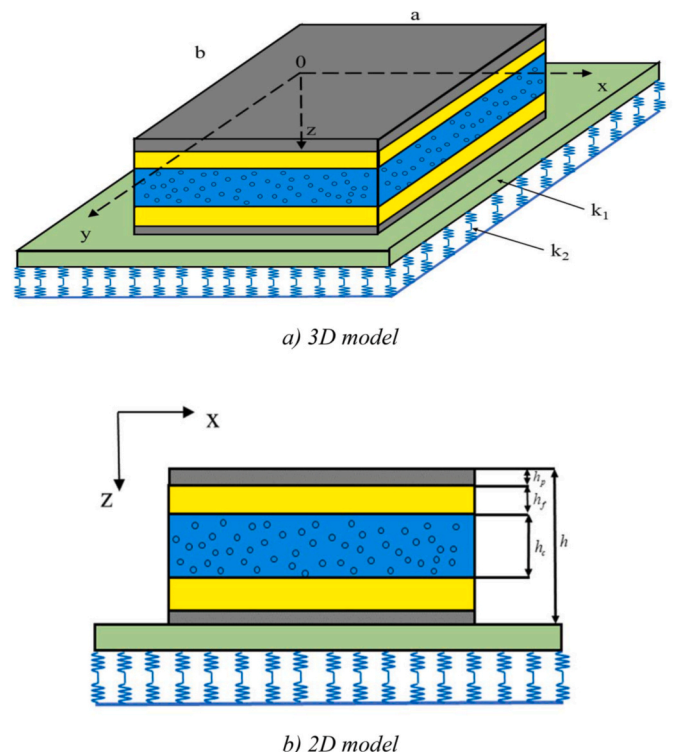


Fig. 1. Schematic diagram of a smart sandwich plate on elastic foundations.

To the best of authors' knowledge, there is no investigation on the nonlinear thermal dynamic buckling and geometrical optimization of smart sandwich plate which is composed of a porous homogeneous core, two carbon nanotube reinforced composite layers and two piezoelectric face sheets subjected to mechanical, thermal and electric loadings. The novelty and significant contributions of the paper may be expressed as

$$\lambda(z) = \begin{cases} \cos(\pi z/h_c) & \text{Non-uniform symmetric distribution} \\ \cos(\pi z/2h_c + \pi/4) & \text{Non-uniform asymmetric distribution} \\ \lambda_0 & \text{Uniform distribution} \end{cases} \quad (3)$$

follows:

- It is the first time that the model of smart sandwich plate with five layers including porous core, CNTRC layers and piezoelectric face sheets is introduced.
- The material properties of porous homogenous core and two CNTRC layers are assumed to depend on temperature.
- Based on the analytical approach, the clear expression for frequency, critical dynamic buckling load, deflection amplitude – time and frequency ratio – amplitude relations are obtained, which are the input basis (objective functions) for optimization problems.
- The optimum values of geometrical and material parameters of smart sandwich plate corresponding to maximum value of natural frequency are obtained by using Bees Algorithm.
- The effect of material and geometrical parameters, elastic foundations as well as external impacts are considered in details, which provide scientific basis for designers and engineering in the specific objectives.

## 2. Modeling and material properties of the proposed smart sandwich plate

As shown in Fig. 1, a smart sandwich plate with total thickness  $h$ , length  $a$  and width  $b$  is considered. The Cartesian coordinates  $(x, y, z)$  is located on the middle surface of the plate in which  $z$  is in thickness direction. The smart sandwich plate consists of five layers; which has functionally graded porous homogeneous core, two carbon nanotube reinforced composite layers and two piezoelectric face sheets. The thickness of core layer, each carbon nanotube reinforced composite layer and each piezoelectric face sheet are  $h_c$ ,  $h_f$  and  $h_p$ , respectively. The displacement components in the middle surface to the coordinates  $(x, y, z)$  are  $u, v$  and  $w$ , respectively, and  $\varphi_x, \varphi_y$  denote respectively the rotations of the transverse normal about the  $y$  and  $x$  axes at  $z = 0$ .

The smart sandwich plate is assumed to rest on Pasternak-type elastic foundations. The interaction between the sandwich plate and elastic foundations is modeled by a Winkler independent spring system with modulus  $k_1$  and a Pasternak shear layer with stiffness  $k_2$ . Further, the smart sandwich plate is subjected to an external pressure  $q$  uniformly distributed on the surface of the plate.

The Young's modulus  $E^c$ , mass density  $\rho^c$  and thermal expansion coefficients  $\alpha^c$  of porous core are assumed to be location-dependent as (Ansari et al., 2020; Xue et al., 2019)

$$\begin{aligned} E^c &= E_1[1 - e_0\lambda(z)], \\ \rho^c &= \rho_1[1 - e_m\lambda(z)], \\ \alpha^c &= \alpha_1[1 - e_m\lambda(z)], \end{aligned} \quad (1)$$

where  $E_1, \rho_1, \alpha_1$  are material properties of non-porous original material of core layer;  $e_0$  and  $e_m$  are the coefficient of porosity and the mass density coefficient, respectively. The relationship between  $e_0$  and  $e_m$  can be given as

$$e_m = 1 - \sqrt{1 - e_0} \quad (0 \leq e_0 \leq 1). \quad (2)$$

Three different types of porosity distributions, namely non-uniform symmetric distribution, non-uniform asymmetric distribution and uniform distribution, are considered. The function  $\lambda(z)$  is expressed in three different cases as (Xue et al., 2019)

in which

$$\lambda_0 = \frac{1}{e_0} - \frac{1}{e_0} \left( \frac{2}{\pi} \sqrt{1 - e_0} - \frac{2}{\pi} + 1 \right)^2. \quad (4)$$

The titanium alloy (Ti-6Al-4V) is chosen for the original material without porosity of core layer. Except the Poisson's ratio and mass density, the elastic modulus of this homogeneous material are assumed to be nonlinear temperature-dependent as (Shen et al., 2017a)

$$\begin{aligned} \nu_1 &= 0.29, \rho_1 = 4429 \text{ kg/m}^3, \\ \alpha_1 &= 7.5788(1 + 6.638 \times 10^{-4}T + 3.147 \times 10^{-6}T^2) \times 10^{-6} /K, \\ E_1 &= 122.56(1 - 4.586 \times 10^{-4}T) \text{ GPa}, \end{aligned} \quad (5)$$

in which  $T = T_0 + \Delta T$ ,  $T_0$  is the room temperature and  $\Delta T$  is the temperature increment in the environment containing the material.

The FG-CNTRC material is composed of homogeneous matrix reinforced by (10,10) single-walled carbon nanotubes (SWCNTs). The effective Young's modulus, shear modulus, Poisson's ratio, mass density and the longitudinal and transverse thermal expansion coefficients of the FG-CNTRC material are expressed as (Shen et al., 2017a)

$$\begin{aligned} E_{11} &= \eta_1 V_{CNT} E_{11}^{CNT} + V_m E_m, \\ \frac{\eta_2}{E_{22}} &= \frac{V_{CNT}}{E_{22}^{CNT}} + \frac{V_m}{E_m}, \\ \frac{\eta_3}{G_{12}} &= \frac{V_{CNT}}{G_{12}^{CNT}} + \frac{V_m}{G_m}, \\ G_{13} &= G_{12}, \quad G_{23} = 1.2G_{12}, \\ \nu_{12} &= V_{CNT}^* \nu_{12}^{CNT} + V_m \nu_m, \\ \rho &= V_{CNT} \rho_{CNT} + V_m \rho_m, \\ \alpha_{11} &= \frac{V_{CNT} E_{11}^{CNT} \alpha_{11}^{CNT} + V_m E_m \alpha_m}{V_{CNT} E_{11}^{CNT} + V_m E_m}, \\ \alpha_{22} &= (1 + \nu_{12}^{CNT}) V_{CNT} \alpha_{22}^{CNT} + (1 + \nu_m) V_m \alpha_m - \nu_{12} \alpha_{11}, \end{aligned} \quad (6)$$

where the subscript and superscript CNT and  $m$  denote carbon nanotube and homogeneous matrix components, respectively.  $V_{CNT}$  and  $V_m$  are the volume fractions of the carbon nanotube and the matrix, respectively and  $\eta_i$  ( $i = \overline{1, 3}$ ) are the CNT efficiency parameters which are determined by matching the effective material properties of FG-CNTRC obtained from molecular simulation results with those from the rule of mixtures (Shen et al., 2013, 2014, 2017a, 2017bbib\_Shen\_and\_Wang\_2017abib\_Shen\_et\_al\_2017bbib\_Shen\_and\_Xiang\_2013bib\_Shen\_and\_Xiang\_2014).

In this study, it is assumed that the volume fractions of the CNTs and homogeneous matrix distribute according to linear functions throughout the thickness direction for top and bottom layers as

**Table 1**  
The domain of nine variables of global optimization.

Variable	Domain
$h_c$ (m)	$[10^{-3}, 10^{-1}]$
$h_f$ (m)	$[10^{-3}, 10^{-1}]$
$h_p$ (m)	$[10^{-3}, 10^{-1}]$
$a$ (m)	$[0.05, 5]$
$b$ (m)	$[0.05, 5]$
$k_1$ (Pa/m)	$[0, 0.9 \times 10^9]$
$k_2$ (Pa.m)	$[0, 0.9 \times 10^9]$
$\Delta T$ (K)	$[0, 1000]$
$e_0$	$[0, 1]$

$$V_{CNT}(z) = \begin{cases} 2((z - h_c/2)/h_f) V_{CNT}^* & \text{Top face} \\ 2((-h_c/2 - z)/h_f) V_{CNT}^* & \text{Bottom face} \end{cases} \quad (7)$$

$$V_m(z) = 1 - V_{CNT}(z),$$

where

$$V_{CNT}^* = \frac{w_{CNT}}{w_{CNT} + (\rho_{CNT}/\rho_m) - (\rho_{CNT}/\rho_m)w_{CNT}}, \quad (8)$$

in which  $w_{CNT}$  is the mass fraction of CNTs.

Except Poisson's ratio, the material properties of the CNT and homogeneous matrix are assumed to strongly depend on temperature as (Shen et al., 2017a, 2017bbib\_Shen\_and\_Wang\_2017abib\_Shen\_et\_al\_2017b)

$$\nu_m = 0.34,$$

$$E_m = (3.52 - 0.0034T) \text{ GPa}, \alpha_m = 45(1 + 0.0005\Delta T) \times 10^{-6} /K,$$

$$\nu_{12}^{CNT} = 0.175,$$

$$E_{11}^{CNT} = (6.18387 - 0.00286T + 4.22867 \times 10^{-6}T^2 - 2.2724 \times 10^{-9}T^3) \text{ (TPa)},$$

$$E_{22}^{CNT} = (7.75348 - 0.00358T + 5.30057 \times 10^{-6}T^2 - 2.84868 \times 10^{-9}T^3) \text{ (TPa)}, \quad (9)$$

$$G_{12}^{CNT} = (1.80126 - 7.7845 \times 10^{-4}T - 1.1279 \times 10^{-6}T^2 + 4.93484 \times 10^{-9}T^3) \text{ (TPa)},$$

$$\alpha_{11}^{CNT} = (-1.12148 + 0.02289T - 2.88155 \times 10^{-5}T^2 + 1.13253 \times 10^{-8}T^3) (\times 10^{-6}/K),$$

$$\alpha_{22}^{CNT} = (5.43874 - 9.95498 \times 10^{-4}T + 3.13525 \times 10^{-7}T^2 - 3.36332 \times 10^{-12}T^3) (\times 10^{-6}/K).$$

### 3. Fundamental equations

The Reddy's higher order shear deformation plate theory is used to establish basic equations and investigate the nonlinear vibration and dynamic buckling analysis of the smart sandwich plate.

#### 3.1. Strain field

For small strains and moderate deflection, the strain field of the smart sandwich plate are defined as (Reddy, 2004; Brush and Almoth, 1975)

$$\begin{bmatrix} \epsilon_x \\ \epsilon_y \\ \gamma_{xy} \end{bmatrix} = \begin{bmatrix} \epsilon_x^0 \\ \epsilon_y^0 \\ \gamma_{xy}^0 \end{bmatrix} + z \begin{bmatrix} k_x^1 \\ k_y^1 \\ k_{xy}^1 \end{bmatrix} + z^3 \begin{bmatrix} k_x^3 \\ k_y^3 \\ k_{xy}^3 \end{bmatrix}, \quad \begin{bmatrix} \gamma_{xz} \\ \gamma_{yz} \end{bmatrix} = \begin{bmatrix} \gamma_{xz}^0 \\ \gamma_{yz}^0 \end{bmatrix} + z^2 \begin{bmatrix} k_{xz}^2 \\ k_{yz}^2 \end{bmatrix}, \quad (10)$$

where

$$\begin{bmatrix} \epsilon_x^0 \\ \epsilon_y^0 \\ \gamma_{xy}^0 \end{bmatrix} = \begin{bmatrix} \frac{\partial u}{\partial x} + \frac{1}{2} \left( \frac{\partial w}{\partial x} \right)^2 \\ \frac{\partial v}{\partial y} + \frac{1}{2} \left( \frac{\partial w}{\partial y} \right)^2 \\ \frac{\partial u}{\partial y} + \frac{\partial v}{\partial x} + \frac{\partial w}{\partial x} \frac{\partial w}{\partial y} \end{bmatrix}, \quad \begin{bmatrix} \gamma_{xz}^0 \\ \gamma_{yz}^0 \end{bmatrix} = -3c_1 \begin{bmatrix} \frac{\partial w}{\partial x} + \varphi_x \\ \frac{\partial w}{\partial y} + \varphi_y \end{bmatrix}, \quad \begin{bmatrix} k_x^1 \\ k_y^1 \\ k_{xy}^1 \end{bmatrix} \\ = \begin{bmatrix} \frac{\partial \varphi_x}{\partial x} \\ \frac{\partial \varphi_y}{\partial y} \\ \frac{\partial \varphi_x}{\partial y} + \frac{\partial \varphi_y}{\partial x} \end{bmatrix}, \quad \begin{bmatrix} k_x^3 \\ k_y^3 \\ k_{xy}^3 \end{bmatrix} = -c_1 \begin{bmatrix} \frac{\partial \varphi_x}{\partial x} + \frac{\partial^2 w}{\partial x^2} \\ \frac{\partial \varphi_y}{\partial y} + \frac{\partial^2 w}{\partial y^2} \\ \frac{\partial \varphi_x}{\partial y} + \frac{\partial \varphi_y}{\partial x} + 2 \frac{\partial^2 w}{\partial x \partial y} \end{bmatrix}, \quad \begin{bmatrix} k_{xz}^2 \\ k_{yz}^2 \end{bmatrix} \\ = -3c_1 \begin{bmatrix} \frac{\partial w}{\partial x} + \varphi_x \\ \frac{\partial w}{\partial y} + \varphi_y \end{bmatrix}, \quad (11)$$

with  $c_1 = 4/(3h^2)$ .

#### 3.2. Stress – strain relations

The stress field of the functionally graded porous homogeneous core is given as follows

$$\begin{bmatrix} \sigma_{xx} \\ \sigma_{yy} \\ \sigma_{xy} \\ \sigma_{xz} \\ \sigma_{yz} \end{bmatrix}_C = \begin{bmatrix} Q_{11}^C & Q_{12}^C & 0 & 0 & 0 \\ Q_{12}^C & Q_{22}^C & 0 & 0 & 0 \\ 0 & 0 & Q_{66}^C & 0 & 0 \\ 0 & 0 & 0 & Q_{44}^C & 0 \\ 0 & 0 & 0 & 0 & Q_{55}^C \end{bmatrix} \begin{bmatrix} (\epsilon_{xx})_C - \alpha^C \Delta T \\ (\epsilon_{yy})_C - \alpha^C \Delta T \\ (\epsilon_{xy})_C \\ (\epsilon_{xz})_C \\ (\epsilon_{yz})_C \end{bmatrix}, \quad (12)$$

in which elastic stiffness are

$$Q_{11}^C = Q_{22}^C = \frac{E^C}{1 - (\nu^C)^2}, \quad Q_{12}^C = \frac{\nu^C E^C}{1 - (\nu^C)^2}, \quad Q_{66}^C = Q_{44}^C = Q_{55}^C = \frac{E^C}{2(1 + \nu^C)}. \quad (13)$$

For carbon nanotube reinforced composite layers, the linear constitutive relation is expressed by Hooke's law as

$$\begin{bmatrix} \sigma_{xx} \\ \sigma_{yy} \\ \sigma_{xy} \\ \sigma_{xz} \\ \sigma_{yz} \end{bmatrix}_f = \begin{bmatrix} Q_{11}^f & Q_{12}^f & 0 & 0 & 0 \\ Q_{12}^f & Q_{22}^f & 0 & 0 & 0 \\ 0 & 0 & Q_{66}^f & 0 & 0 \\ 0 & 0 & 0 & Q_{44}^f & 0 \\ 0 & 0 & 0 & 0 & Q_{55}^f \end{bmatrix} \begin{bmatrix} (\epsilon_{xx})_f - \alpha_{11}\Delta T \\ (\epsilon_{yy})_f - \alpha_{22}\Delta T \\ (\epsilon_{xy})_f \\ (\epsilon_{xz})_f \\ (\epsilon_{yz})_f \end{bmatrix}, \quad (14)$$

where

$$Q_{11}^f = \frac{E_{11}}{1 - \nu_{12}\nu_{21}}, \quad Q_{22}^f = \frac{E_{22}}{1 - \nu_{12}\nu_{21}}, \quad Q_{12}^f = \frac{\nu_{21}E_{11}}{1 - \nu_{12}\nu_{21}}, \quad Q_{44}^f = G_{23}, \quad Q_{55}^f = G_{13}, \quad Q_{66}^f = G_{12}. \quad (15)$$

By taking into account the effect of temperature and electric field, the stress-strain relation of isotropic piezoelectric face sheets can be written as

$$\begin{bmatrix} \sigma_{xx} \\ \sigma_{yy} \\ \sigma_{xy} \\ \sigma_{xz} \\ \sigma_{yz} \end{bmatrix}_p = \begin{bmatrix} Q_{11}^p & Q_{12}^p & 0 & 0 & 0 \\ Q_{12}^p & Q_{22}^p & 0 & 0 & 0 \\ 0 & 0 & Q_{66}^p & 0 & 0 \\ 0 & 0 & 0 & Q_{44}^p & 0 \\ 0 & 0 & 0 & 0 & Q_{55}^p \end{bmatrix} \begin{bmatrix} (\epsilon_{xx})_p - \alpha^p \Delta T \\ (\epsilon_{yy})_p - \alpha^p \Delta T \\ (\epsilon_{xy})_p \\ (\epsilon_{xz})_p \\ (\epsilon_{yz})_p \end{bmatrix} - \begin{bmatrix} 0 & 0 & e_{31} \\ 0 & 0 & e_{32} \\ 0 & e_{24} & 0 \\ e_{15} & 0 & 0 \\ 0 & 0 & 0 \end{bmatrix} \begin{bmatrix} E_x \\ E_y \\ E_z \end{bmatrix}, \quad (16)$$

in which

$$Q_{11}^p = Q_{22}^p = \frac{E^p}{1 - (\nu^p)^2}, \quad Q_{12}^p = \frac{\nu^p E^p}{1 - (\nu^p)^2}, \quad Q_{66}^p = Q_{44}^p = Q_{55}^p = \frac{E^p}{2(1 + \nu^p)}, \quad (17)$$

and  $e_{31}, e_{32}, e_{15}, e_{24}$  are the piezoelectric stiffness of piezoelectric layers which can be determined from dielectric constants  $d_{31}, d_{32}, d_{15}, d_{24}$  and elastic stiffness as

$$\begin{aligned} e_{31} &= d_{31}Q_{11}^p + d_{32}Q_{12}^p, \\ e_{32} &= d_{31}Q_{12}^p + d_{32}Q_{22}^p, \\ e_{15} &= d_{15}Q_{55}^p, \\ e_{24} &= d_{24}Q_{44}^p. \end{aligned} \quad (18)$$

$$\begin{aligned} &-c_{1j16} \left( \frac{\partial^2 w}{\partial y^2} + \frac{\partial \varphi_y}{\partial y} \right) + j_{17} (\Phi_1 + 2V_p e_{31}) + j_{18} (\Phi_2 + 2V_p e_{32}), \\ \epsilon_y^0 &= j_{21} \frac{\partial^2 f}{\partial x^2} - j_{12} \frac{\partial^2 f}{\partial y^2} + j_{23} \frac{\partial \varphi_x}{\partial x} + j_{24} \frac{\partial \varphi_y}{\partial y} - c_{1j25} \left( \frac{\partial^2 w}{\partial x^2} + \frac{\partial \varphi_x}{\partial x} \right) - c_{1j26} \left( \frac{\partial^2 w}{\partial y^2} + \frac{\partial \varphi_y}{\partial y} \right) + j_{27} (\Phi_1 + 2V_p e_{31}) + j_{28} (\Phi_2 + 2V_p e_{32}), \\ \gamma_{xy}^0 &= -j_{31} \frac{\partial^2 f}{\partial x \partial y} + j_{32} \left( \frac{\partial \varphi_x}{\partial y} + \frac{\partial \varphi_y}{\partial x} \right) - c_{1j33} \left( 2 \frac{\partial^2 w}{\partial x \partial y} + \frac{\partial \varphi_x}{\partial y} + \frac{\partial \varphi_y}{\partial x} \right), \end{aligned} \quad (22)$$

In this study, we assume that the piezoelectric polarization is along  $z$  direction. Therefore, the components of electric field are expressed as

$$[E_x \ E_y \ E_z]^T = [0 \ 0 \ V_p/h_p]^T, \quad (19)$$

with  $V_p$  is applied voltage to the piezoelectric layers in the thickness direction.

### 3.3. Force and moment components

By integrating the stress through the thickness, the force and moment resultants of the smart sandwich plate can be determined as

$$\begin{aligned} (N_i, M_i, P_i) &= \sum_{k=1}^5 \int_{z_k}^{z_{k+1}} \sigma_i^k(1, z, z^3) dz, \quad i = x, y, xy \\ (Q_i, R_i) &= \sum_{k=1}^5 \int_{z_k}^{z_{k+1}} \sigma_{iz}^k(1, z^2) dz, \quad i = x, y, \end{aligned} \quad (20)$$

in which  $z_k$  and  $z_{k+1}$  are the coordinates of the  $k$ th layer of the smart sandwich plate.

By substituting Eq. (10) into Eqs. (12), (14) and (16) then obtained results into Eq. (20), the force and moment – strain relationship of the smart sandwich plate can be written as

$$\begin{aligned} N_x &= A_{11}\epsilon_x^0 + A_{12}\epsilon_y^0 + B_{11}k_x^1 + B_{12}k_y^1 + E_{11}k_x^3 + E_{12}k_y^3 - \Phi_1 - 2V_a e_{31}, \\ N_y &= A_{12}\epsilon_x^0 + A_{22}\epsilon_y^0 + B_{12}k_x^1 + B_{22}k_y^1 + E_{12}k_x^3 + E_{22}k_y^3 - \Phi_2 - 2V_a e_{32}, \\ N_{xy} &= A_{66}\epsilon_{xy}^0 + B_{66}k_{xy}^1 + E_{66}k_{xy}^3, \\ M_x &= B_{11}\epsilon_x^0 + B_{12}\epsilon_y^0 + D_{11}k_x^1 + D_{12}k_y^1 + F_{11}k_x^3 + F_{12}k_y^3 - \Phi_3, \\ M_y &= B_{12}\epsilon_x^0 + B_{22}\epsilon_y^0 + D_{12}k_x^1 + D_{22}k_y^1 + F_{12}k_x^3 + F_{22}k_y^3 - \Phi_4, \\ M_{xy} &= B_{66}\epsilon_{xy}^0 + D_{66}k_{xy}^1 + F_{66}k_{xy}^3, \\ P_x &= E_{11}\epsilon_x^0 + E_{12}\epsilon_y^0 + F_{11}k_x^1 + F_{12}k_y^1 + H_{11}k_x^3 + H_{12}k_y^3 - \Phi_5, \\ P_y &= E_{12}\epsilon_x^0 + E_{22}\epsilon_y^0 + F_{12}k_x^1 + F_{22}k_y^1 + H_{12}k_x^3 + H_{22}k_y^3 - \Phi_6, \\ P_{xy} &= E_{66}\epsilon_{xy}^0 + F_{66}k_{xy}^1 + H_{66}k_{xy}^3, \\ Q_x &= A_{44}\gamma_{xz}^0 + D_{44}k_{xz}^2, \quad Q_y = A_{55}\gamma_{yz}^0 + D_{55}k_{yz}^2, \\ R_x &= D_{44}\gamma_{xz}^0 + F_{44}k_{xz}^2, \quad R_y = D_{55}\gamma_{yz}^0 + F_{55}k_{yz}^2, \end{aligned} \quad (21)$$

in which the detail of coefficients  $A_{ij}, B_{ij}, D_{ij}, E_{ij}, F_{ij}, H_{ij}$  ( $ij = 11, 12, 22$ ),  $A_{kl}, D_{kl}, F_{kl}$  ( $kl = 44, 55$ ),  $\Phi_m$  ( $m = 1, 2, 3, 4, 5, 6$ ) may be found in Appendix A.

The strain components in the middle surface of the smart sandwich plate can be obtained from Eq. (21) as follows

$$\begin{aligned} \epsilon_x^0 &= j_{11} \frac{\partial^2 f}{\partial y^2} - j_{12} \frac{\partial^2 f}{\partial x^2} + j_{13} \frac{\partial \varphi_x}{\partial x} + j_{14} \frac{\partial \varphi_y}{\partial y} - c_{1j15} \left( \frac{\partial^2 w}{\partial x^2} + \frac{\partial \varphi_x}{\partial x} \right) \\ &- c_{1j16} \left( \frac{\partial^2 w}{\partial y^2} + \frac{\partial \varphi_y}{\partial y} \right) + j_{17} (\Phi_1 + 2V_p e_{31}) + j_{18} (\Phi_2 + 2V_p e_{32}), \\ \epsilon_y^0 &= j_{21} \frac{\partial^2 f}{\partial x^2} - j_{12} \frac{\partial^2 f}{\partial y^2} + j_{23} \frac{\partial \varphi_x}{\partial x} + j_{24} \frac{\partial \varphi_y}{\partial y} - c_{1j25} \left( \frac{\partial^2 w}{\partial x^2} + \frac{\partial \varphi_x}{\partial x} \right) - c_{1j26} \left( \frac{\partial^2 w}{\partial y^2} + \frac{\partial \varphi_y}{\partial y} \right) + j_{27} (\Phi_1 + 2V_p e_{31}) + j_{28} (\Phi_2 + 2V_p e_{32}), \\ \gamma_{xy}^0 &= -j_{31} \frac{\partial^2 f}{\partial x \partial y} + j_{32} \left( \frac{\partial \varphi_x}{\partial y} + \frac{\partial \varphi_y}{\partial x} \right) - c_{1j33} \left( 2 \frac{\partial^2 w}{\partial x \partial y} + \frac{\partial \varphi_x}{\partial y} + \frac{\partial \varphi_y}{\partial x} \right), \end{aligned} \quad (22)$$

where

$$\begin{aligned} \Delta &= A_{11}A_{22} - A_{12}^2, \quad j_{11} = \frac{A_{22}}{\Delta}, \quad j_{12} = \frac{A_{12}}{\Delta}, \quad j_{13} = \frac{B_{12}A_{12} - B_{11}A_{22}}{\Delta}, \\ j_{14} &= \frac{B_{22}A_{12} - B_{12}A_{22}}{\Delta}, \quad j_{15} = \frac{E_{12}A_{12} - E_{11}A_{22}}{\Delta}, \quad j_{16} = \frac{E_{22}A_{12} - E_{12}A_{22}}{\Delta}, \end{aligned}$$

$$j_{17} = \frac{A_{22}}{\Delta}, j_{18} = -\frac{A_{12}}{\Delta}, j_{21} = \frac{A_{11}}{\Delta}, j_{23} = \frac{B_{11}A_{12} - B_{12}A_{11}}{\Delta}, j_{24} = \frac{B_{12}A_{12} - B_{22}A_{11}}{\Delta}, j_{25} = \frac{E_{11}A_{12} - E_{12}A_{11}}{\Delta}, \quad (23)$$

$$j_{26} = \frac{E_{12}A_{12} - E_{22}A_{11}}{\Delta}, j_{27} = -\frac{A_{12}}{\Delta}, j_{28} = \frac{A_{11}}{\Delta}, j_{31} = \frac{1}{A_{66}}, j_{32} = -\frac{B_{66}}{A_{66}},$$

$$j_{33} = \frac{E_{66}}{A_{66}}.$$

and the Airy's stress function  $f(x, y, t)$  is defined as

$$N_x = \frac{\partial^2 f}{\partial y^2}, N_y = \frac{\partial^2 f}{\partial x^2}, N_{xy} = -\frac{\partial^2 f}{\partial x \partial y}. \quad (24)$$

### 3.4. Motion and geometrical compatibility equations

Based on the Hamilton principle and the basis of Reddy's higher order shear deformation plate theory, the nonlinear motion equation of the smart sandwich plate are defined as (Reddy, 2004; Brush and Almqvist, 1975)

$$\frac{\partial N_x}{\partial x} + \frac{\partial N_{xy}}{\partial y} = \bar{J}_1 \frac{\partial^2 u}{\partial t^2} + \bar{J}_2 \frac{\partial^2 \varphi_x}{\partial t^2} - \bar{J}_3 \frac{\partial^3 w}{\partial t^2 \partial x}, \quad (25a)$$

$$\frac{\partial N_{xy}}{\partial x} + \frac{\partial N_y}{\partial y} = \bar{J}_1^* \frac{\partial^2 v}{\partial t^2} + \bar{J}_2^* \frac{\partial^2 \varphi_y}{\partial t^2} - \bar{J}_3^* \frac{\partial^3 w}{\partial t^2 \partial y}, \quad (25b)$$

$$\begin{aligned} \frac{\partial Q_x}{\partial x} + \frac{\partial Q_y}{\partial y} - 3c_1 \left( \frac{\partial R_x}{\partial x} + \frac{\partial R_y}{\partial y} \right) + c_1 \left( \frac{\partial^2 P_x}{\partial x^2} + 2 \frac{\partial^2 P_y}{\partial x \partial y} + \frac{\partial^2 P_y}{\partial y^2} \right) + q + N_x \frac{\partial^2 w}{\partial x^2} \\ + 2N_{xy} \frac{\partial^2 w}{\partial x \partial y} + N_y \frac{\partial^2 w}{\partial y^2} - k_1 w + k_2 \nabla^2 w = J_1 \frac{\partial^2 w}{\partial t^2} + 2\epsilon J_1 \frac{\partial w}{\partial t} + \bar{J}_3 \frac{\partial^3 u}{\partial t^2 \partial x} + \bar{J}_3 \frac{\partial^3 \varphi_x}{\partial t^2 \partial x} \\ + \bar{J}_3^* \frac{\partial^3 v}{\partial t^2 \partial y} + \bar{J}_3^* \frac{\partial^3 \varphi_y}{\partial t^2 \partial y} - c_1^2 J_7 \left( \frac{\partial^4 w}{\partial t^2 \partial x^2} + \frac{\partial^4 w}{\partial t^2 \partial y^2} \right), \end{aligned} \quad (25c)$$

$$\frac{\partial M_x}{\partial x} + \frac{\partial M_{xy}}{\partial y} - Q_x + 3c_1 R_x - c_1 \left( \frac{\partial P_x}{\partial x} + \frac{\partial P_{xy}}{\partial y} \right) = \bar{J}_2 \frac{\partial^2 u}{\partial t^2} + \bar{J}_4 \frac{\partial^2 \varphi_x}{\partial t^2} - \bar{J}_5 \frac{\partial^3 w}{\partial t^2 \partial x}, \quad (25d)$$

$$\frac{\partial M_{xy}}{\partial x} + \frac{\partial M_y}{\partial y} - Q_y + 3c_1 R_y - c_1 \left( \frac{\partial P_{xy}}{\partial x} + \frac{\partial P_y}{\partial y} \right) = \bar{J}_2^* \frac{\partial^2 v}{\partial t^2} + \bar{J}_4^* \frac{\partial^2 \varphi_y}{\partial t^2} - \bar{J}_5^* \frac{\partial^3 w}{\partial t^2 \partial y}, \quad (25e)$$

in which  $\epsilon$  is the viscous damping coefficient and

$$\bar{J}_1 = J_1, \bar{J}_2 = J_2 - c_1 J_4, \bar{J}_3 = c_1 J_4, \bar{J}_4 = J_3 - 2c_1 J_5 + c_1^2 J_7, \bar{J}_5 = c_1 J_5 - c_1^2 J_7,$$

$$\frac{\partial^2 u}{\partial t^2} = -\frac{\bar{J}_2}{\bar{J}_1} \frac{\partial^2 \varphi_x}{\partial t^2} + \frac{\bar{J}_3}{\bar{J}_1} \frac{\partial^3 w}{\partial t^2 \partial x}, \quad (27a)$$

$$\frac{\partial^2 v}{\partial t^2} = -\frac{\bar{J}_2^*}{\bar{J}_1^*} \frac{\partial^2 \varphi_y}{\partial t^2} + \frac{\bar{J}_3^*}{\bar{J}_1^*} \frac{\partial^3 w}{\partial t^2 \partial y}. \quad (27b)$$

Now substituting Eqs. (27a) and (27b) into Eq. (25c) – (25e), the differential system equations can be obtained as follows

$$\begin{aligned} \frac{\partial Q_x}{\partial x} + \frac{\partial Q_y}{\partial y} - 3c_1 \left( \frac{\partial R_x}{\partial x} + \frac{\partial R_y}{\partial y} \right) + c_1 \left( \frac{\partial^2 P_x}{\partial x^2} + 2 \frac{\partial^2 P_{xy}}{\partial x \partial y} + \frac{\partial^2 P_y}{\partial y^2} \right) + \frac{\partial^2 f}{\partial y^2} \frac{\partial^2 w}{\partial x^2} \\ - 2 \frac{\partial^2 f}{\partial x \partial y} \frac{\partial^2 w}{\partial x \partial y} + \frac{\partial^2 f}{\partial x^2} \frac{\partial^2 w}{\partial y^2} + q - k_1 w + k_2 \nabla^2 w + \frac{1}{R_x} \frac{\partial^2 f}{\partial x^2} + \frac{1}{R_y} \frac{\partial^2 f}{\partial y^2} \\ = J_1 \frac{\partial^2 w}{\partial t^2} + 2\epsilon J_1 \frac{\partial w}{\partial t} + \bar{J}_3 \frac{\partial^3 \varphi_x}{\partial t^2 \partial x} + \bar{J}_3^* \frac{\partial^3 \varphi_y}{\partial t^2 \partial y} + \bar{J}_7 \frac{\partial^4 w}{\partial t^2 \partial x^2} + \bar{J}_7^* \frac{\partial^4 w}{\partial t^2 \partial y^2}, \end{aligned} \quad (28a)$$

$$\frac{\partial M_x}{\partial x} + \frac{\partial M_{xy}}{\partial y} - Q_x + 3c_1 R_x - c_1 \left( \frac{\partial P_x}{\partial x} + \frac{\partial P_{xy}}{\partial y} \right) = \bar{J}_3 \frac{\partial^2 \varphi_x}{\partial t^2} - \bar{J}_5 \frac{\partial^3 w}{\partial t^2 \partial x}, \quad (28b)$$

$$\frac{\partial M_{xy}}{\partial x} + \frac{\partial M_y}{\partial y} - Q_y + 3c_1 R_y - c_1 \left( \frac{\partial P_{xy}}{\partial x} + \frac{\partial P_y}{\partial y} \right) = \bar{J}_3^* \frac{\partial^2 \varphi_y}{\partial t^2} - \bar{J}_5^* \frac{\partial^3 w}{\partial t^2 \partial y}, \quad (28c)$$

in which

$$\begin{aligned} \bar{J}_3 = \bar{J}_4 - \left( \bar{J}_2 \right)^2 / \bar{J}_1, \bar{J}_3^* = \bar{J}_4^* - \left( \bar{J}_2^* \right)^2 / \bar{J}_1^*, \bar{J}_5 = \bar{J}_5 - \bar{J}_2 \bar{J}_3 / \bar{J}_1, \bar{J}_5^* = \bar{J}_5^* - \bar{J}_2^* \bar{J}_3^* / \bar{J}_1^* \\ = \bar{J}_5^* - \bar{J}_2^* \bar{J}_3^* / \bar{J}_1^* \bar{J}_7 = \left( \bar{J}_3 \right)^2 / \bar{J}_1 - c_1^2 J_7, \bar{J}_7^* = \left( \bar{J}_3^* \right)^2 / \bar{J}_1^* - c_1^2 J_7. \end{aligned} \quad (29)$$

By substituting Eq. (22) into Eq. (21) and the results into Eq. (28) leads to

$$\begin{aligned} L_{11}(w) + L_{12}(\varphi_x) + L_{13}(\varphi_y) + L_{14}(f) + S(w, f) + q = J_1 \frac{\partial^2 w}{\partial t^2} + 2\epsilon J_1 \frac{\partial w}{\partial t} + \bar{J}_3 \frac{\partial^3 \varphi_x}{\partial t^2 \partial x} \\ + \bar{J}_3^* \frac{\partial^3 \varphi_y}{\partial t^2 \partial y} + \bar{J}_7 \frac{\partial^4 w}{\partial t^2 \partial x^2} + \bar{J}_7^* \frac{\partial^4 w}{\partial t^2 \partial y^2}, \\ L_{21}(w) + L_{22}(\varphi_x) + L_{23}(\varphi_y) + L_{24}(f) = \bar{J}_3 \frac{\partial^2 \varphi_x}{\partial t^2} - \bar{J}_5 \frac{\partial^3 w}{\partial t^2 \partial x}, \\ L_{31}(w) + L_{32}(\varphi_x) + L_{33}(\varphi_y) + L_{34}(f) = \bar{J}_3^* \frac{\partial^2 \varphi_y}{\partial t^2} - \bar{J}_5^* \frac{\partial^3 w}{\partial t^2 \partial y}. \end{aligned} \quad (30)$$

where

$$L_{11}(w) = O_{11} \frac{\partial^2 w}{\partial x^2} + O_{12} \frac{\partial^2 w}{\partial y^2} + O_{13} \frac{\partial^4 w}{\partial x^4} + O_{14} \frac{\partial^4 w}{\partial x^2 \partial y^2} + O_{15} \frac{\partial^4 w}{\partial y^4}$$

$$\begin{aligned} (J_1, J_2, J_3, J_4, J_5, J_7) = \int_{-hc/2}^{hc/2} \rho_c(z) (1, z, z^2, z^3, z^4, z^6) dz + \int_{-hf-hc/2}^{-hf-hc/2} \rho_p(z) (1, z, z^2, z^3, z^4, z^6) dz + \int_{-hf-hc/2}^{-hc/2} \rho_f(z) (1, z, z^2, z^3, z^4, z^6) dz \\ + \int_{hc/2}^{hc/2+hf} \rho_f(z) (1, z, z^2, z^3, z^4, z^6) dz + \int_{hc/2+hf}^{hc/2+hf+hp} \rho_p(z) (1, z, z^2, z^3, z^4, z^6) dz. \end{aligned} \quad (26)$$

By replacing Eq. (22) into two first equations of system Eq. (25), we can collect the second derivative of the displacements with respect to time as

$$\begin{aligned}
 & -k_1 w + k_2 \left( \frac{\partial^2 w}{\partial x^2} + \frac{\partial^2 w}{\partial y^2} \right), L_{12}(\varphi_x) = O_{11} \frac{\partial \varphi_x}{\partial x} + O_{16} \frac{\partial^3 \varphi_x}{\partial x^3} + X O_{17} \frac{\partial^3 \varphi_x}{\partial x \partial y^2}, \\
 L_{13}(\varphi_y) &= O_{12} \frac{\partial \varphi_y}{\partial y} + O_{18} \frac{\partial^3 \varphi_y}{\partial y^3} + O_{19} \frac{\partial^3 \varphi_y}{\partial x^2 \partial y}, \\
 L_{14}(f) &= O_{110} \frac{\partial^4 f}{\partial x^4} + O_{111} \frac{\partial^4 f}{\partial x^2 \partial y^2} + O_{112} \frac{\partial^4 f}{\partial y^4}, \\
 S(w, f) &= \frac{\partial^2 f}{\partial y^2} \frac{\partial^2 w}{\partial x^2} - 2 \frac{\partial^2 f}{\partial x \partial y} \frac{\partial^2 w}{\partial y^2} + \frac{\partial^2 f}{\partial x^2} \frac{\partial^2 w}{\partial y^2}, \\
 L_{21}(w) &= O_{21} \frac{\partial w}{\partial x} + O_{22} \frac{\partial^3 w}{\partial x^3} + O_{23} \frac{\partial^3 w}{\partial x \partial y^2}, L_{22}(\varphi_x) = O_{21} \varphi_x + O_{24} \frac{\partial^2 \varphi_x}{\partial x^2} + O_{25} \frac{\partial^2 \varphi_x}{\partial y^2}, \\
 L_{31}(w) &= O_{31} \frac{\partial w}{\partial y} + O_{32} \frac{\partial^3 w}{\partial x^2 \partial y} + O_{33} \frac{\partial^3 w}{\partial y^3}, L_{32}(\varphi_x) = O_{34} \frac{\partial^2 \varphi_x}{\partial x \partial y}, \\
 L_{33}(\varphi_y) &= O_{31} \varphi_y + O_{35} \frac{\partial^2 \varphi_y}{\partial x^2} + O_{36} \frac{\partial^2 \varphi_y}{\partial y^2}, L_{34}(f) = O_{37} \frac{\partial^3 f}{\partial x^2 \partial y} + O_{38} \frac{\partial^3 f}{\partial y^3}, \quad (31)
 \end{aligned}$$

and the detail of coefficients  $O_{1i}(i = \overline{1, 12})$ ,  $O_{2j}(j = \overline{1, 8})$ ,  $O_{3k}(k = \overline{1, 8})$  are given in Appendix B.

Because of errors in manufacturing, transportation and storage process; the geometrical imperfection may exist in the smart sandwich plate. This initial imperfection is represented by function  $w^*(x, y)$  which is assumed to be small compared to the deflection of the sandwich plate. The motion equations of the imperfect smart sandwich plate can be rewritten as

$$\begin{aligned}
 & L_{11}(w) + L_{12}(\varphi_x) + L_{13}(\varphi_y) + L_{14}(f) + S(w, f) + L_{11}^*(w^*) + S^*(w^*, f) \\
 & + q = J_1 \frac{\partial^2 w}{\partial t^2} + 2\epsilon J_1 \frac{\partial w}{\partial t} + \overline{J_5} \frac{\partial^3 \varphi_x}{\partial t^2 \partial x} + \overline{J_5} \frac{\partial^3 \varphi_y}{\partial t^2 \partial y} + \overline{J_7} \frac{\partial^4 w}{\partial t^2 \partial x^2} + \overline{J_7} \frac{\partial^4 w}{\partial t^2 \partial y^2}, \\
 & L_{21}(w) + L_{22}(\varphi_x) + L_{23}(\varphi_y) + L_{24}(f) + L_{21}^*(w^*) \\
 & = \overline{J_3} \frac{\partial^2 \varphi_x}{\partial t^2} - \overline{J_5} \frac{\partial^3 w}{\partial t^2 \partial x}, L_{31}(w) + L_{32}(\varphi_x) + L_{33}(\varphi_y) + L_{34}(f) + L_{31}^*(w^*) \\
 & = \overline{J_3} \frac{\partial^2 \varphi_y}{\partial t^2} - \overline{J_5} \frac{\partial^3 w}{\partial t^2 \partial y}, \quad (32)
 \end{aligned}$$

where

$$\begin{aligned}
 L_{11}^*(w^*) &= O_{11} \frac{\partial^2 w^*}{\partial x^2} + O_{12} \frac{\partial^2 w^*}{\partial y^2}, S^*(w^*, f) = \frac{\partial^2 f}{\partial y^2} \frac{\partial^2 w^*}{\partial x^2} - 2 \frac{\partial^2 f}{\partial x \partial y} \frac{\partial^2 w^*}{\partial y^2} \\
 & + \frac{\partial^2 f}{\partial x^2} \frac{\partial^2 w^*}{\partial y^2}, L_{21}^*(w^*) = O_{21} \frac{\partial w^*}{\partial x}, L_{31}^*(w^*) = O_{31} \frac{\partial w^*}{\partial y}, \quad (33)
 \end{aligned}$$

In order to find the displacements of the sandwich plate, we need to use one equation which shows the relationship of the strain components. Specifically, the geometrical compatibility equation for an imperfect smart sandwich plate is introduced as (Dat et al., 2020)

$$\begin{aligned}
 \frac{\partial^2 \epsilon_x^0}{\partial y^2} + \frac{\partial^2 \epsilon_y^0}{\partial x^2} - \frac{\partial^2 \gamma_{xy}^0}{\partial x \partial y} &= \frac{\partial^2 w^2}{\partial x \partial y} - \frac{\partial^2 w}{\partial x^2} \frac{\partial^2 w}{\partial y^2} + 2 \frac{\partial^2 w}{\partial x \partial y} \frac{\partial^2 w^*}{\partial x \partial y} - \frac{\partial^2 w}{\partial x^2} \frac{\partial^2 w^*}{\partial y^2} \\
 & - \frac{\partial^2 w}{\partial y^2} \frac{\partial^2 w^*}{\partial x^2}, \quad (34)
 \end{aligned}$$

Inserting Eq. (22) into Eq. (34), the compatibility equation of the imperfect sandwich plate becomes

$$\begin{aligned}
 & j_{21} \frac{\partial^4 f}{\partial x^4} + j_{11} \frac{\partial^4 f}{\partial y^4} + H_1 \frac{\partial^4 f}{\partial x^2 \partial y^2} + H_2 \frac{\partial^3 \varphi_x}{\partial x^3} + H_3 \frac{\partial^3 \varphi_x}{\partial x \partial y^2} + H_4 \frac{\partial^3 \varphi_y}{\partial y^3} \\
 & + H_5 \frac{\partial^3 \varphi_y}{\partial y \partial x^2} - c_{1j25} \frac{\partial^4 w}{\partial x^4} - c_{1j16} \frac{\partial^4 w}{\partial y^4} + j_6 \frac{\partial^4 w}{\partial x^2 \partial y^2} \\
 & - \left( \frac{\partial^2 w^2}{\partial x \partial y} - \frac{\partial^2 w}{\partial x^2} \frac{\partial^2 w}{\partial y^2} + 2 \frac{\partial^2 w}{\partial x \partial y} \frac{\partial^2 w^*}{\partial x \partial y} - \frac{\partial^2 w}{\partial x^2} \frac{\partial^2 w^*}{\partial y^2} - \frac{\partial^2 w}{\partial y^2} \frac{\partial^2 w^*}{\partial x^2} - \frac{1}{R} \frac{\partial^2 w}{\partial x^2} \right) = 0, \quad (35)
 \end{aligned}$$

in which

$$\begin{aligned}
 H_1 &= j_{31} - 2j_{12}, H_2 = j_{23} - c_{1j25}, H_3 = j_{13} - c_{1j13} - j_{32} + c_{1j33}, \\
 H_4 &= j_{14} - c_{1j16}, H_5 = j_{24} - c_{1j26} - j_{32} + c_{1j33}, H_6 = -c_{1j15} - c_{1j26} + 2c_{1j33}. \quad (36)
 \end{aligned}$$

By using basic differential equations (32) and (35), the nonlinear vibration and dynamic buckling of the imperfect smart sandwich plate are considered based on Reddy's higher order shear deformation plate theory.

#### 4. Nonlinear dynamic analysis

##### 4.1. Boundary conditions and solution forms

Four edges of the smart sandwich plate are assumed to be simply supported and immovable. The boundary conditions are given as

$$\begin{aligned}
 x = 0, a : w = u = \varphi_y = M_x = P_x = 0, N_x = N_{x0}, \\
 y = 0, b : w = v = \varphi_x = M_y = P_y = 0, N_y = N_{y0}, \quad (37)
 \end{aligned}$$

in which  $N_{x0}$  and  $N_{y0}$  are fictitious compressive edge loads of the sandwich plate.

The deflection and rotations of the smart sandwich plate are defined in terms of unknown time-dependent coefficients and one term mode shapes based on boundary conditions as follows (Duc et al., 2019; Dat et al., 2020)

$$\begin{bmatrix} w(x, y, t) \\ \varphi_x(x, y, t) \\ \varphi_y(x, y, t) \end{bmatrix} = \begin{bmatrix} W(t) \sin \lambda_m x \sin \delta_n y \\ \Phi_x(t) \cos \lambda_m x \sin \delta_n y \\ \Phi_y(t) \sin \lambda_m x \cos \delta_n y \end{bmatrix}, \quad (38)$$

where  $\lambda_m = m\pi/a$ ,  $\delta_n = n\pi/b$  with  $m, n$  are number of half sine and cosine waves and responsible for denoting the mode shape of the sandwich plate;  $W$ ,  $\Phi_x$  and  $\Phi_y$  are time-dependent amplitude of the deflection and rotation angles.

For initial geometrical imperfection, we assume that function  $w^*$  can be expressed by multiplication of spatial terms as

$$w^*(x, y, t) = W_0 \sin \lambda_m x \sin \delta_n y, \quad (39)$$

where  $W_0$  is amplitude of the initial imperfect function.

By substituting Eqs. (38) and (39) into Eq. (35) and balancing coefficients on both sides, the stress function is determined as

$$f(x, y, t) = C_1(t) \cos 2\lambda_m x + C_2(t) \cos 2\delta_n y + C_3(t) \sin \lambda_m x \sin \delta_n y + \frac{1}{2} N_{y0} x^2 + \frac{1}{2} N_{x0} y^2, \quad (40)$$

where

$$C_1 = \frac{\delta_n^2}{32I_{21}\lambda_m^2} W(W + 2\mu h), C_2 = \frac{\lambda_m^2}{32I_{11}\delta_n^2} W(W + 2\mu h), C_3 = G_1 W + G_2 \Phi_x + G_3 \Phi_y, \quad (41)$$

and

$$G_1 = \frac{c_{1j25}\lambda_m^4 + c_{1j16}\delta_n^4 - H_6\lambda_m^2\delta_n^2}{j_{21}\lambda_m^4 + H_1\lambda_m^2\delta_n^2 + j_{11}\delta_n^4}, G_2 = \frac{-(H_2\lambda_m^3 + H_3\lambda_m\delta_n^2)}{j_{21}\lambda_m^4 + H_1\lambda_m^2\delta_n^2 + j_{11}\delta_n^4}, \quad (42)$$

$$G_3 = \frac{-(H_4\delta_n^3 + H_5\lambda_m^2\delta_n)}{j_{21}\lambda_m^4 + H_1\lambda_m^2\delta_n^2 + j_{11}\delta_n^4}.$$

Substituting Eq. (38) – (40) into equation (32) then applying Galerkin method for obtained equations, we obtain the nonlinear system of differential equations to investigate the nonlinear vibration and dynamic buckling of smart sandwich plate with porous core, CNTRC layers and piezoelectric face sheets as

$$\begin{aligned}
 & l_{11}W + l_{12}\Phi_x + l_{13}\Phi_y + l_{14}(W + W_0)\Phi_x + l_{15}(W + W_0)\Phi_y + [n_1 - N_{x0}\lambda_m^2 - N_{y0}\delta_n^2](W + W_0) + n_2W(W + W_0) + n_3W(W + 2W_0) + n_4W(W + W_0)(W + 2W_0) + n_5q \\
 & = J_0 \frac{\partial^2 W}{\partial t^2} + 2\varepsilon J_1 \frac{\partial W}{\partial t} - \lambda_m J_5 \frac{\partial^2 \Phi_x}{\partial t^2} - \delta_n J_5 \frac{\partial^2 \Phi_y}{\partial t^2}, l_{21}W + l_{22}\Phi_x + l_{23}\Phi_y + n_6(W + W_0) + n_7W(W + 2W_0) \\
 & = J_3 \frac{\partial^2 \Phi_x}{\partial t^2} - \lambda_m J_5 \frac{\partial^2 W}{\partial t^2}, l_{31}W + l_{32}\Phi_x + l_{33}\Phi_y + n_8(W + W_0) + n_9W(W + 2W_0) = J_3 \frac{\partial^2 \Phi_y}{\partial t^2} - \delta_n J_5 \frac{\partial^2 W}{\partial t^2},
 \end{aligned} \tag{43}$$

in which the details of coefficients  $l_{1i}(i = \overline{1, 3}), l_{jk}(j = \overline{2, 3}, k = \overline{1, 2}), n_m(m = \overline{1, 9})$  may be found in Appendix C.

#### 4.2. Vibration and dynamic buckling analysis

In order to ensure the existence of thermal stresses and consider the effect of temperature on the vibration of the smart sandwich plate, four edges of the plate are assumed to be immovable in the transverse plane. In other words, displacement components are eliminated in four edges, i. e.  $u = 0$  on  $x = 0, a$  and  $v = 0$  on  $y = 0, b$ . These conditions are satisfied on the average sense on the whole area of the plate surface as (Duc et al., 2019; Dat et al., 2020)

$$\int_0^b \int_0^a \frac{\partial u}{\partial x} dx dy = 0, \int_0^a \int_0^b \frac{\partial v}{\partial x} dy dx = 0, \tag{44}$$

The derivative of the displacement components can be obtained by substituting Eq. (22) into Eq. (11) as

$$\begin{aligned}
 \frac{\partial u}{\partial x} & = j_{11} \frac{\partial^2 f}{\partial y^2} - j_{12} \frac{\partial^2 f}{\partial x^2} + j_{13} \frac{\partial \varphi_x}{\partial x} + j_{14} \frac{\partial \varphi_y}{\partial y} - c_{1j15} \left( \frac{\partial^2 w}{\partial x^2} + \frac{\partial \varphi_x}{\partial x} \right) - c_{1j16} \left( \frac{\partial^2 w}{\partial y^2} + \frac{\partial \varphi_y}{\partial y} \right) + j_{17}(\Phi_1 + 2V_p e_{31}) + j_{18}(\Phi_2 + 2V_p e_{32}) - \frac{1}{2} \left( \frac{\partial w}{\partial x} \right)^2 - \frac{\partial w}{\partial x} \frac{\partial w^*}{\partial x}, \\
 \frac{\partial v}{\partial y} & = j_{21} \frac{\partial^2 f}{\partial x^2} - j_{12} \frac{\partial^2 f}{\partial y^2} + j_{23} \frac{\partial \varphi_x}{\partial x} + j_{24} \frac{\partial \varphi_y}{\partial y} - c_{1j25} \left( \frac{\partial^2 w}{\partial x^2} + \frac{\partial \varphi_x}{\partial x} \right) - c_{1j26} \left( \frac{\partial^2 w}{\partial y^2} + \frac{\partial \varphi_y}{\partial y} \right) + j_{27}(\Phi_1 + 2V_p e_{31}) + j_{28}(\Phi_2 + 2V_p e_{32}) - \frac{1}{2} \left( \frac{\partial w}{\partial y} \right)^2 - \frac{\partial w}{\partial y} \frac{\partial w^*}{\partial y}.
 \end{aligned} \tag{45}$$

$$\begin{aligned}
 a_1 & = -j_{11}\delta_n^2 G_1 + j_{12}G_1\lambda_m^2 + c_{1j15}\lambda_m^2 + c_{1j16}\delta_n^2, a_2 = (-j_{13} + c_{1j15})\lambda_m + j_{12}G_2\lambda_m^2 - j_{11}G_2\delta_n^2, a_3 = (-j_{14} + c_{1j16})\delta_n + G_3j_{12}\lambda_m^2 - j_{11}G_3\delta_n^2, \\
 a_4 & = -G_1j_{21}\lambda_m^2 + \delta_n^2 G_1j_{12} + c_{1j26}\delta_n^2 + c_{1j25}\lambda_m^2, a_5 = (-j_{23} + c_{1j25})\lambda_m + j_{12}G_2\delta_n^2 - j_{21}G_2\lambda_m^2, a_6 = (-j_{24} + c_{1j26})\delta_n + j_{12}G_3\delta_n^2 - j_{21}G_3\lambda_m^2.
 \end{aligned} \tag{48}$$

Replacing Eq. (38) – (40) into Eq. (45) then substituting the obtained results into Eq. (44), the fictitious compressive edge loads are expressed to depend on the amplitude of the deflection and rotation angles as

$$\begin{aligned}
 N_{x0} & = g_1W + g_4(W + W_0)W + g_2\Phi_x + g_3\Phi_y + g_5(\Phi_1 + 2V_p e_{31}) + g_6(\Phi_2 + 2V_p e_{32}), \\
 N_{y0} & = f_1W + f_4(W + W_0)W + f_2\Phi_x + f_3\Phi_y + f_5(\Phi_1 + 2V_p e_{31}) + f_6(\Phi_2 + 2V_p e_{32}),
 \end{aligned} \tag{46}$$

in which

$$\begin{aligned}
 g_1 & = \frac{(j_{21}a_1 + j_{12}a_4)}{ab(j_{12}^2 - j_{11}j_{21})} \frac{4}{\lambda_m \delta_n}, g_4 = -\frac{1}{8} \frac{(j_{21}\lambda_m^2 + j_{12}\delta_n^2)}{(j_{12}^2 - j_{11}j_{21})}, g_2 = \frac{(j_{21}a_2 + j_{12}a_5)}{ab(j_{12}^2 - j_{11}j_{21})} \frac{4}{\lambda_m \delta_n}, \\
 g_3 & = \frac{(j_{21}a_3 + j_{12}a_6)}{ab(j_{12}^2 - j_{11}j_{21})} \frac{4}{\lambda_m \delta_n}, g_5 = \frac{(j_{17}j_{21} + j_{27}j_{12})}{(j_{12}^2 - j_{11}j_{21})}, g_6 = \frac{(j_{18}j_{21} + j_{28}j_{12})}{(j_{12}^2 - j_{11}j_{21})}, \\
 f_1 & = \frac{(a_1j_{12} + j_{11}a_4)}{ab(j_{12}^2 - j_{11}j_{21})} \frac{4}{\lambda_m \delta_n}, f_4 = -\frac{1}{8} \frac{(\lambda_m^2 j_{12} + j_{11} \delta_n^2)}{(j_{12}^2 - j_{11}j_{21})}, f_2 = \frac{(a_2j_{12} + j_{11}a_5)}{ab(j_{12}^2 - j_{11}j_{21})} \frac{4}{\lambda_m \delta_n}, \\
 f_3 & = \frac{(a_3j_{12} + j_{11}a_6)}{ab(j_{12}^2 - j_{11}j_{21})} \frac{4}{\lambda_m \delta_n}, f_5 = \frac{(j_{17}j_{12} + j_{11}j_{27})}{(j_{12}^2 - j_{11}j_{21})}, f_6 = \frac{(j_{18}j_{12} + j_{11}j_{28})}{(j_{12}^2 - j_{11}j_{21})},
 \end{aligned} \tag{47}$$

and

Substituting Eq. (46) into Eq. (43) and assuming that the external pressure is a linear function of time  $q = st$ , the nonlinear system of differential equations becomes

$$\begin{aligned}
 & l_{11}W + l_{12}\Phi_x + l_{13}\Phi_y + l_{14}^1(W + W_0)\Phi_x + l_{15}^1(W + W_0)\Phi_y + n_1^1(W + W_0) \\
 & + n_2^1W(W + W_0) + n_3W(W + 2W_0) + n_4^1W(W + W_0)(W + 2W_0) + n_5st \\
 & = J_0 \frac{\partial^2 W}{\partial t^2} + 2\varepsilon J_1 \frac{\partial W}{\partial t} - \lambda_m J_5 \frac{\partial^2 \Phi_x}{\partial t^2} - \delta_n J_5 \frac{\partial^2 \Phi_y}{\partial t^2}, l_{21}W + l_{22}\Phi_x + l_{23}\Phi_y \\
 & + n_6(W + W_0) + n_7W(W + 2W_0) \\
 & = J_3 \frac{\partial^2 \Phi_x}{\partial t^2} - \lambda_m J_5 \frac{\partial^2 W}{\partial t^2}, l_{31}W + l_{32}\Phi_x + l_{33}\Phi_y + n_8(W + W_0) \\
 & + n_9W(W + 2W_0) \\
 & = J_3 \frac{\partial^2 \Phi_y}{\partial t^2} - \delta_n J_5 \frac{\partial^2 W}{\partial t^2},
 \end{aligned} \tag{49}$$

where

$$\begin{aligned}
 l_{14}^1 &= (l_{14} - \lambda_m^2 g_2 - \delta_n^2 f_2), l_{15}^1 = (l_{15} - \lambda_m^2 g_3 - \delta_n^2 f_3), \\
 n_1^1 &= \begin{bmatrix} n_1 - (\lambda_m^2 g_5 + \delta_n^2 f_5)(\Phi_1 + 2V_p e_{31}) \\ -(\lambda_m^2 g_6 + \delta_n^2 f_6)(\Phi_2 + 2V_p e_{32}) \end{bmatrix}, \\
 n_2^1 &= (n_2 - \lambda_m^2 g_1 - \delta_n^2 f_1), n_4^1 = (n_4 - \lambda_m^2 g_4 - \delta_n^2 f_4).
 \end{aligned}
 \tag{50}$$

By using the fourth – order Runge – Kutta method, the nonlinear dynamic response, the values of natural frequency and the relation between frequency ratio and amplitude of the smart sandwich plate with simply supported edges is obtained from Eq. (49) in which the initial conditions are chosen to be  $W(0) = \Phi_x(0) = \Phi_y(0) = \frac{dW}{dt}(0) = \frac{d\Phi_x}{dt}(0) = \frac{d\Phi_y}{dt}(0) = 0$ . For dynamic buckling, Budiansky – Roth criterion (Budiansky and Roth, 1962) is used to determine the dynamic critical time  $t_{dcr}$ . Specifically, the dynamic critical time can be selected at any point during the period at which the deflection – time curve changes suddenly to the first maximum value.

The natural frequencies of the perfect smart sandwich plate is determined by solving the following equation in which the minimum value of three solutions is chosen

$$\begin{aligned}
 & \left| \begin{array}{cccc} l_{11} + n_1^1 + J_0 \omega^2 & l_{12} - \lambda_m \bar{J}_5 \omega^2 l_{13} - \delta_n \bar{J}_5 \omega^2 l_{21} + n_6 - \lambda_m \bar{J}_5 \omega^2 l_{22} & & \\ & & & \\ & & & \\ & & & \end{array} \right| \\
 & + \bar{J}_3 \omega^2 l_{23} l_{31} + n_8 - \delta_n \bar{J}_5 \omega^2 l_{32} l_{33} + \bar{J}_3 \omega^2 = 0.
 \end{aligned}
 \tag{51}$$

In fact, the inertial forces caused by the rotation angles are small compared to the inertial forces caused by the deflection. Therefore, we can ignore two inertial forces  $\frac{\partial^2 \Phi_x}{\partial t^2}$ ,  $\frac{\partial^2 \Phi_y}{\partial t^2}$  and Eq. (49) can be rewritten as

$$\begin{aligned}
 & l_{11}W + l_{12}\Phi_x + l_{13}\Phi_y + l_{14}(W + \mu h)\Phi_x + l_{15}(W + \mu h)\Phi_y + n_1^1(W + \mu h) \\
 & + n_2^1W(W + \mu h) + n_3W(W + 2\mu h) + n_4^1W(W + \mu h)(W + 2\mu h) + n_5q \\
 & = J_0 \frac{\partial^2 W}{\partial t^2} + 2\epsilon J_1 \frac{\partial W}{\partial t}, l_{21}W + l_{22}\Phi_x + l_{23}\Phi_y + n_6(W + \mu h) + n_7W(W + 2\mu h) \\
 & = -\lambda_m \bar{J}_5 \frac{\partial^2 W}{\partial t^2}, l_{31}W + l_{32}\Phi_x + l_{33}\Phi_y + n_8(W + \mu h) + n_9W(W + 2\mu h) \\
 & = -\delta_n \bar{J}_5 \frac{\partial^2 W}{\partial t^2}.
 \end{aligned}
 \tag{52}$$

The uniformly distributed transverse load is assumed to be in form of  $q = Q \sin \Omega t$  in which  $Q$  is the amplitude and  $\Omega$  is the frequency. We can collect the rotation angles amplitude  $\Phi_x$  and  $\Phi_y$  from the last two equations of system Eq. (52) then replacing the obtained results into first equation of system Eq. (52) yields

**Table 2**  
The values of parameters of standard Bees Algorithm.

Parameter	Value
Number of scout bees	25
Number of elite bees	3
Number of best bees	8
Number of recruited bees around each elite bee	20
Number of recruited bees around each best bee	10
initial size of neighbourhood	0.08
Number of limit loop for site abandonment	10

**Table 3**

Comparison of the non-dimensional natural frequencies  $\tilde{\omega} = 2h\omega\sqrt{2\rho(1+\nu)/E}$  of the homogeneous plate with  $a/b = 2$ ,  $a/h = 24$ ,  $40$ .

Mode	a/h	Source		
		Farsangi et al. (2013)	Srinivas et al. (1970)	Present
(1,1)	40	0.0589	0.0589	0.0585
	24	0.1576	0.1581	0.1567
(2,1)	40	0.0930	0.0931	0.0924
	24	0.2444	0.2455	0.2431
(3,1)	40	0.1481	0.1485	0.1472
	24	0.3788	0.3811	0.3771
(4,1)	40	0.2218	0.2226	0.2206
	24	0.5497	0.5544	0.5480

**Table 4**

Comparison of the dimensionless natural frequencies of CNTRC plates  $\tilde{\omega} = \Omega(a^2/h)\sqrt{\rho_m/E_m}$  with  $m = n = 1$ ,  $a/b = 1$ ,  $b/h = 50$ ,  $T = 300K$ .

$V_{CNT}^*$	Types	Zhu et al. (2012)	Shen and Wang (2017a)	Present
0.11	FG-O	14.302	14.138	14.264
	FG-X	22.984	23.143	23.024
0.14	FG-O	15.801	15.667	15.796
	FG-X	25.555	25.831	25.670
0.17	FG-O	17.544	17.351	17.506
	FG-X	28.413	28.625	28.421

$$\begin{aligned}
 & \left[ \bar{J}_0 - J_0^*(W + \mu h) \right] \frac{d^2 W}{dt^2} + 2\epsilon J_1 \frac{dW}{dt} - s_{11}W - s_{12}(W + \mu h) \\
 & - s_{13}W(W + \mu h) - s_{14}W(W + 2\mu h) - s_{15}(W + \mu h)^2 \\
 & - s_{16}W(W + \mu h)(W + 2\mu h) = n_5 Q \sin \Omega t,
 \end{aligned}
 \tag{53}$$

where the details of coefficients  $\bar{J}_0$ ,  $J_0^*$  and  $s_{1i}(i = \overline{1,6})$  are shown in Appendix D.

For the smart sandwich plate without initial imperfection, Eq. (53) becomes

$$\begin{aligned}
 & \left( \bar{J}_0 - J_0^* W \right) \frac{d^2 W}{dt^2} + 2\epsilon J_1 \frac{dW}{dt} - (s_{11} + s_{12})W \\
 & - (s_{13} + s_{14} + s_{15})W^2 - s_{16}W^3 = n_5 Q \sin \Omega t.
 \end{aligned}
 \tag{54}$$

The coefficient  $J_0^*$  is assumed to be much smaller than coefficient  $\bar{J}_0$  in Eq. (54). By ignoring coefficient  $J_0^*$ , Eq. (54) transform into following form

$$\begin{aligned}
 & \frac{d^2 W}{dt^2} + \frac{2\epsilon J_1}{\bar{J}_0} \frac{dW}{dt} - \frac{(s_{11} + s_{12})}{\bar{J}_0} W \\
 & - \frac{(s_{13} + s_{14} + s_{15})}{\bar{J}_0} W^2 - \frac{s_{16}}{\bar{J}_0} W^3 = \frac{n_5}{\bar{J}_0} Q \sin \Omega t.
 \end{aligned}
 \tag{55}$$

The linear frequency of the smart sandwich plate can be determined by following expression

$$\omega_L = \sqrt{-\frac{(s_{11} + s_{12})}{\bar{J}_0}}.
 \tag{56}$$

By introducing coefficients  $M$ ,  $N$ ,  $P$ , Eq. (55) also can be rewritten as follows

$$\frac{d^2 W}{dt^2} + 2\epsilon \bar{J}_0 \frac{dW}{dt} + \omega_L^2 (W - MW^2 + NW^3) - P \sin \Omega t = 0,
 \tag{57}$$

in which

$$\bar{J}_0^* = \frac{J_1}{\bar{J}_0}, M = -\frac{(s_{13} + s_{14} + s_{15})}{(s_{11} + s_{12})}, N = \frac{s_{16}}{(s_{11} + s_{12})}, P = \frac{n_5 Q}{\bar{J}_0}.
 \tag{58}$$

The amplitude deflection of the smart sandwich plate is assumed to

**Table 5**

Comparison of the non-dimensional frequencies  $\tilde{\omega} = \omega(b/\pi)^2 \sqrt{\rho h/D}$  of square porous steel plates with  $D = E_1 h^3 / [12(1 - \nu^2)]$

Type of porosity distribution		Porosity coefficient $e_0$			
		0.2	0.3	0.4	0.5
Non-uniform symmetric distribution	Present	1.9322	1.9292	1.9284	1.9308
	Xue et al. (2019)	1.9228	1.9210	1.9220	1.9269
Non-uniform asymmetric distribution	Present	1.8860	1.8527	1.8150	1.7707
	Xue et al. (2019)	1.8754	1.8424	1.8050	1.7612
Uniform distribution	Present	1.8778	1.8426	1.8051	1.7651
	Xue et al. (2019)	1.8656	1.8285	1.7877	1.7423

**Table 6**

Effects of porosity coefficient  $e_0$ , temperature increment  $\Delta T$  and CNT volume fraction  $V_{CNT}^*$  on the critical dynamic buckling load (GPa) of the smart sandwich plate with  $a/b = 1$ ,  $b/h = 20$ ,  $h_c/h_f = 5$ ,  $h_c/h_p = 10$ .

$\Delta T$	$V_{CNT}^*$	$e_0$		
		0	0.2	0.4
0	0.12	0.3037	0.3022	0.3002
	0.17	0.3017	0.3001	0.2978
	0.28	0.2983	0.2963	0.2937
100	0.12	0.3056	0.3040	0.3019
	0.17	0.3035	0.3018	0.2994
	0.28	0.3000	0.2979	0.2952
200	0.12	0.3076	0.3060	0.3037
	0.17	0.3055	0.3036	0.3011
	0.28	0.3017	0.2996	0.2967

be in form as  $W(t) = \xi \sin(\omega t)$ . By substituting this form into Eq. (57), the relationship between frequency and amplitude of nonlinear free vibration can be express as

$$\omega_{NL}^2 - 2\varepsilon \bar{J}_0^2 \frac{2\omega_{NL}}{\pi} - \omega_L^2 \left( 1 - M\xi \frac{8}{3\pi} + N\xi^2 \frac{3}{4} \right) = 0. \tag{59}$$

**Table 7**

The effect of types of porosity distribution, width-to-length ratio  $a/b$  and length-to-thickness ratio  $b/h$  on critical dynamic buckling load (GPa) of the smart sandwich plate with  $e_0 = 0.2$ ,  $h_c/h_f = 5$ ,  $V_{CNT}^* = 0.12$ ,  $\Delta T = 100K$ .

Porosity distribution	$a/b$	$b/h = 10$	$b/h = 15$	$b/h = 20$
Non-uniform symmetric porosity	0.5	0.1490	0.2058	0.2373
	1	0.2184	0.2646	0.3040
	1.5	0.2318	0.2849	0.3309
Non-uniform asymmetric porosity	0.5	0.1490	0.2054	0.2370
	1	0.2182	0.2644	0.3038
	1.5	0.2315	0.2847	0.3307
Uniform porosity	0.5	0.1496	0.2058	0.2374
	1	0.2187	0.2647	0.3040
	1.5	0.2320	0.2849	0.3309

**Table 8**

Effects of elastic foundations coefficients  $k_1, k_2$  and the load velocity  $s$  on the critical dynamic buckling load (GPa) of the smart sandwich plate in case of non-uniform symmetric porosity with  $a/b = 1$ ,  $b/h = 20$ ,  $h_c/h_f = 5$ ,  $h_c/h_p = 10$ ,  $\Delta T = 100 K$ .

$(k_1 \text{ (GPa/m)}, k_2 \text{ (GPa.m)})$	$s = 350 \text{ (GPa/s)}$	$s = 700 \text{ (GPa/s)}$	$s = 1000 \text{ (GPa/s)}$
	(0,0)	0.2984	0.5968
(0.3,0)	0.3046	0.6093	0.8704
(0.3,0.04)	0.3053	0.6105	0.8722
(0.5,0.04)	0.3107	0.6213	0.8876

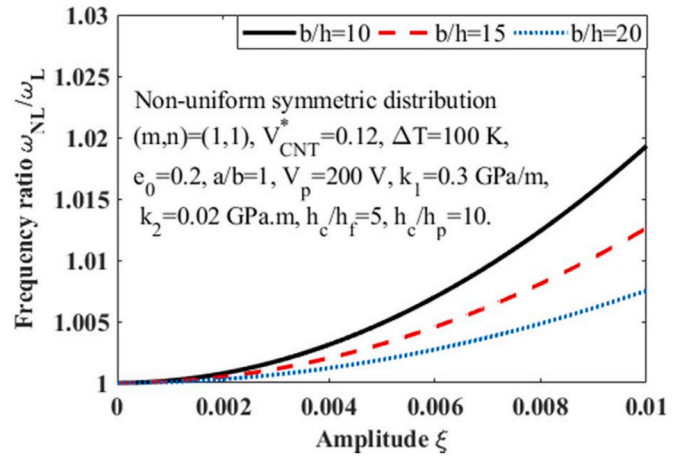


**Fig. 2.** Effects of width-to-thickness ratio  $b/h$  on the frequency ratio – amplitude relation of the smart sandwich plate.

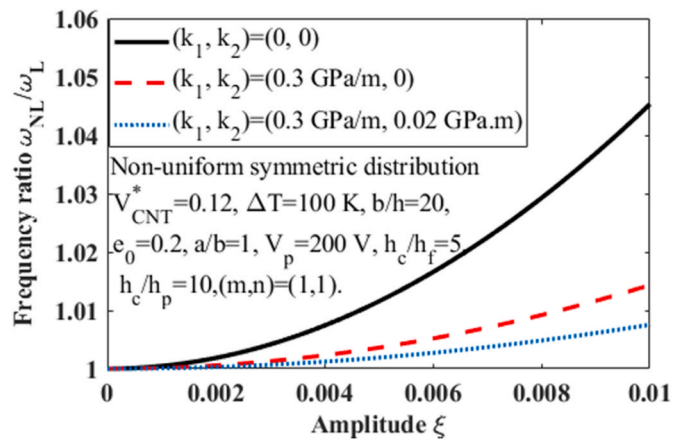


**Fig. 3.** Effects of elastic foundations on the frequency ratio – amplitude relation of the smart sandwich plate.

in which  $\omega_{NL}$  is nonlinear frequency and  $\xi$  is amplitude of free vibration.

### 5. Global optimization

The natural frequency of the smart sandwich plate is determined as Eq. (56). It is assumed to depend on nine geometrical and material

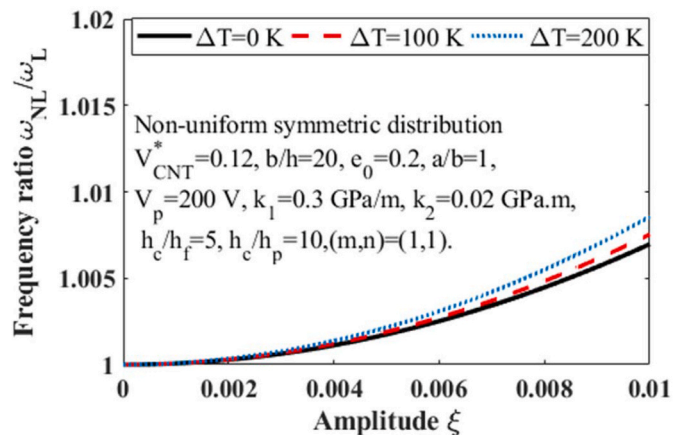


**Fig. 4.** Effects of temperature increment on the frequency ratio – amplitude relation of the smart sandwich plate.

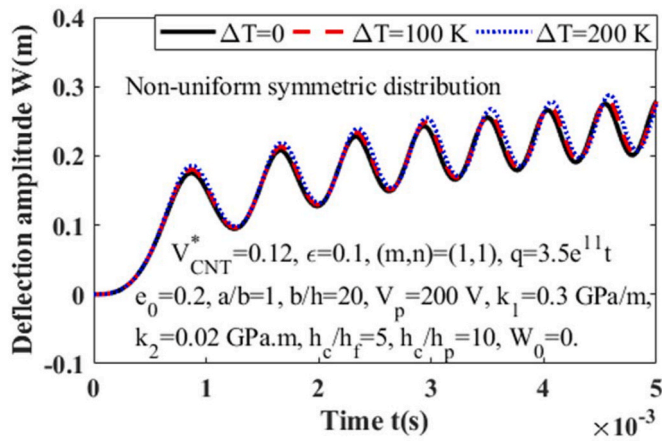


Fig. 5. Effect of temperature increment  $\Delta T$  on the nonlinear dynamic response of the smart sandwich plate.

parameters which are the thickness of porous core, CNTRC layer and piezoelectric face sheet  $h_c, h_f, h_p$ , the length and the width of the plate  $a, b$ , two modulus of elastic foundations  $k_1, k_2$ , the temperature increment  $\Delta T$  and the coefficient of porosity  $e_0$ . The standard Bees Algorithm (Pham et al., 2009) is used to calculate the maximum value of natural frequency and optimum values of above parameters. Nine variables are assumed to be in constant domain as Table 1 and the basic parameters of Bees Algorithm are chosen as Table 2.

## 6. Numerical results and discussions

### 6.1. Comparison studies

Because no existing researches have been carried on the nonlinear vibration of the smart sandwich plates with porous core and CNTRC layers, two comparisons of dimensionless natural frequency of the homogeneous plate and CNTRC plate are presented for validation of the present method.

**Example 1:** In this example, the non-dimensional natural frequencies  $\tilde{\omega} = 2h\omega\sqrt{2\rho(1+\nu)}/E$  of the homogeneous plate are determined and compared with numerical results of Farsangi et al. (2013) based on Mindlin plate theory and analytical results of Srinivas et al. (1970) using a three dimensional linear, small deformation theory of elasticity solution. Four cases of mode number are considered and the material properties are chosen as  $E = 105.7 \text{ GPa}$ ,  $\nu = 0.2981$ ,  $\rho = 4429 \text{ kg/m}^3$ . The geometrical parameters are  $a/b = 2$ ,  $a/h = 24, 40$ . It

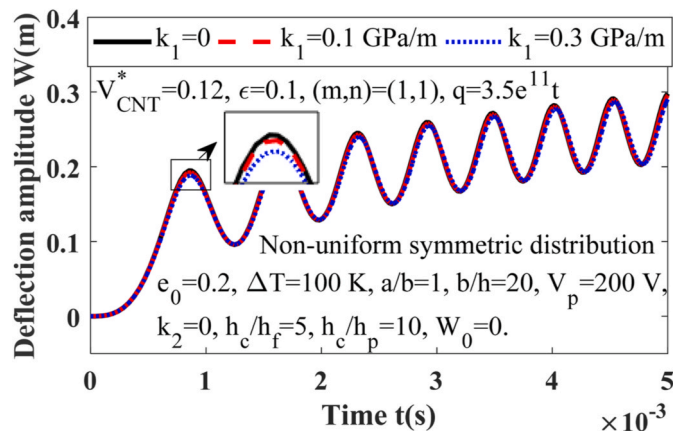


Fig. 6. Effect of the Winkler foundation  $k_1$  on the nonlinear dynamic response of the smart sandwich plate.

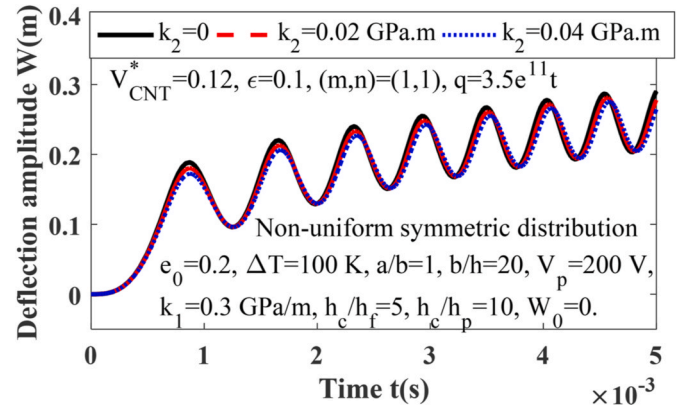


Fig. 7. Effect of the Pasternak foundation  $k_2$  on the nonlinear dynamic response of the smart sandwich plate.

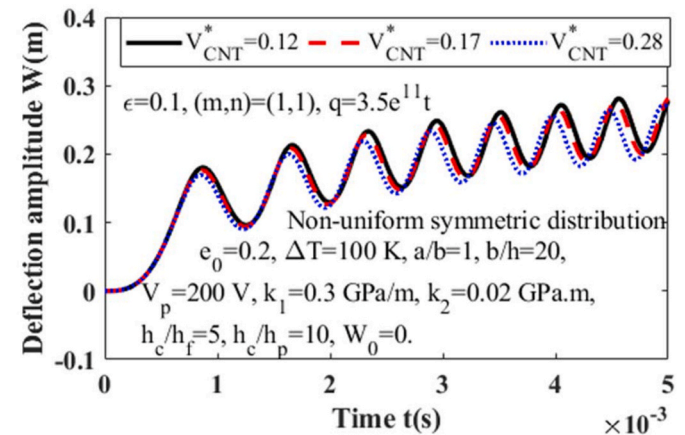


Fig. 8. Effect of CNT volume fraction  $V_{CNT}^*$  on the nonlinear dynamic response of the smart sandwich plate.

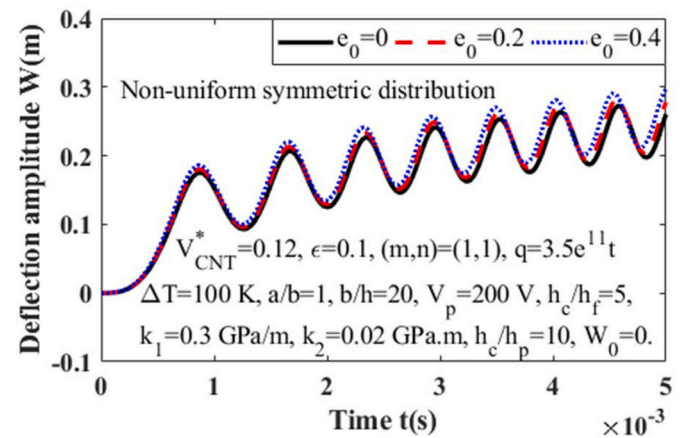


Fig. 9. Effect of porosity coefficient  $e_0$  on the nonlinear dynamic response of the smart sandwich plate.

can be seen from Table 3 that the present results are in good agreement with those obtained by other authors, which shows the reliability and accuracy of present approach and method.

**Example 2:** This example is conducted to indicate the comparison of the dimensionless natural frequencies  $\tilde{\omega} = \Omega(a^2/h)\sqrt{\rho_m/E_m}$  of CNTRC plates with first order shear deformation plate theory results of Zhu et al. (2012) using finite element method and higher order shear deformation

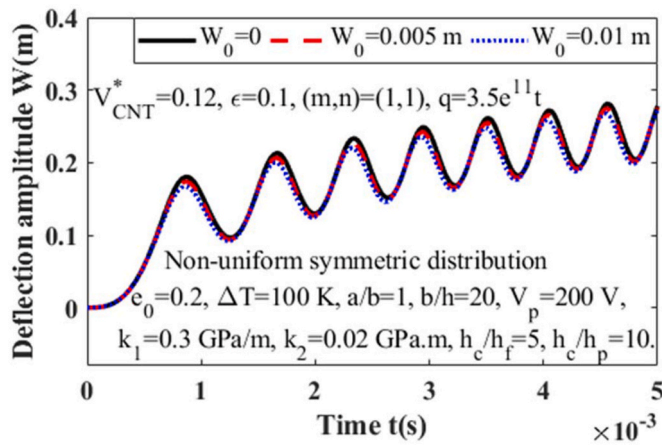


Fig. 10. Effect of initial imperfection amplitude  $W_0$  on the nonlinear dynamic response of the smart sandwich plate.

plate theory results of Shen and Wang (2017) based on analytical approach. The matrix is chosen to be PmPV and the material properties of CNT and the matrix are calculated at  $T = 300\text{ K}$ . Three values of  $V_{CNT}^* = 0.11, 0.14$  and  $0.17$  are considered. It is also evident from Table 4 that the present results reasonable agree with existing results.

**Example 3:** This example illustrates the comparison of the non-dimensional frequencies  $\tilde{\omega} = \omega(b/\pi)^2 \sqrt{\rho h/D}$  ( $D = E_1 h^3 / [12(1 - \nu^2)]$ ) of square porous steel plates between the present results with numerical results of Xue et al. (2019) using isogeometric approach and first order shear deformation theory. The material properties of steel are  $E = 200\text{ GPa}$ ,  $\nu = 0.3$ ,  $\rho = 7850\text{ kg/m}^3$ . The geometrical parameters are taken to be  $a/b = 1$ ,  $b/h = 10$ . Three types of porosity distribution and four values of porosity coefficient are considered in this comparison. The specific evaluation is presented in Table 5, which shows the excellent agreement between two results.

### 6.2. Critical buckling load

Table 6 shows the effect of porosity coefficient  $e_0$ , temperature increment  $\Delta T$  and CNT volume fraction  $V_{CNT}^*$  on the critical dynamic buckling load (GPa) of the smart sandwich plate. The geometrical parameters are chosen to be  $a/b = 1$ ,  $b/h = 20$ ,  $h_c/h_f = 5$ ,  $h_c/h_p = 10$ . The elastic foundations stiffness are taken to be  $k_1 = 0.3\text{ GPa/m}$ ,  $k_2 = 0.02\text{ GPa.m}$ . The results reveal that the critical dynamic buckling load of the smart sandwich plates increases slightly when the temperature

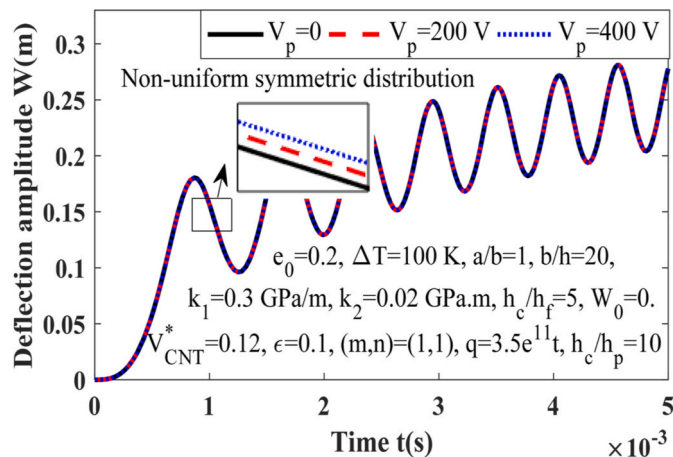


Fig. 11. Effect of the applied voltage  $V_p$  on the nonlinear dynamic response of smart the sandwich plate.

Table 9

The optimum values of nine geometrical and material variables of the smart sandwich plate by using Bees Algorithm.

$h_c$ (m)	0.752
$h_f$ (m)	0.069
$h_p$ (m)	0.027
$a$ (m)	1.49
$b$ (m)	1.03
$k_1$ (Pa/m)	$2.53 \times 10^8$
$k_2$ (Pa.m)	$4.57 \times 10^9$
$\Delta T$ (K)	157.12
$e_0$	0.291

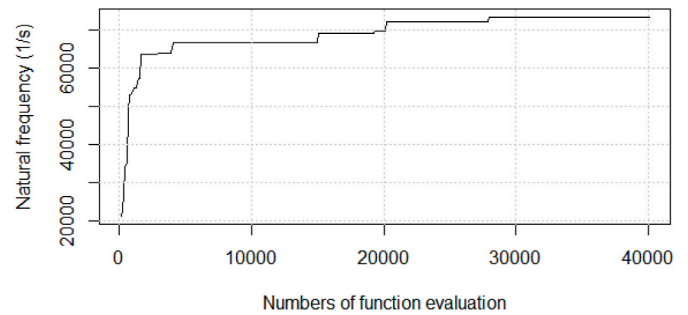


Fig. 12. The convergence of the optimum value of the natural frequency by using Bees Algorithm.

increment  $\Delta T$  increases. Specifically, the critical dynamic buckling load increases from 0.5% to 0.7% when the temperature increment increases 100 K. Conversely, an increase of CNT volume fraction results in a decrease of the critical dynamic buckling load of the sandwich plate. For three values of  $V_{CNT}^* : 0.12, 0.17$  and  $0.28$ , the obtained maximum difference of critical buckling load is 0.8%. This is due to the increase of stress concentrations by adding CNT into polymer matrix. Furthermore, as the increase of porosity coefficient  $e_0$ , the critical dynamic buckling load will become smaller. In other words the porosity has the negative effect on the critical buckling load of the smart sandwich plate. The reason is that the increase of porosity coefficient leads to the reduction of the stiffness of the sandwich plate.

The effects of three types of porosity distribution, width-to-length ratio  $a/b$  ( $= 0.5, 1, 1.5$ ) and length-to-thickness ratio  $b/h$  ( $= 10, 15, 20$ ) on critical dynamic buckling load (GPa) of the smart sandwich plate are presented in Table 7. The input parameters are chosen to be  $e_0 = 0.2$ ,  $h_c/h_f = 5$ ,  $V_{CNT}^* = 0.12$ ,  $\Delta T = 100\text{ K}$ . It can be seen that the critical dynamic buckling load of the plate with uniform porosity distribution is higher than one with non-uniform porosity distribution. Moreover, the difference of the buckling load between two cases of non-uniform porosity is very small and the plate with asymmetric type of porosity distribution has little lower buckling load than one with symmetric type. For width-to-length and length-to-thickness ratios, it is obvious that by the increase of  $a/b$  or  $b/h$  ratio, the critical buckling load rises significantly. For instance, the highest difference with non-uniform symmetric porosity distribution is 8.8% for  $a/b$  ratio and 38% for  $b/h$  ratio. This is due to the enhancement of the stiffness of the plate with the increase of  $a/b$  or  $b/h$  ratio.

Table 8 indicates the effects of elastic foundations coefficients  $k_1$  (GPa/m),  $k_2$  (GPa.m) and the load velocity  $s$  (GPa/s) on the critical dynamic buckling load (GPa) of the smart sandwich plate. The CNT volume fraction is taken to be  $V_{CNT}^* = 0.12$ . The results confirm that the critical dynamic buckling load increase as the elastic foundations coefficients  $k_1$  and  $k_2$  increases. This conclusion can be explained by the

increase of the stiffness of the sandwich plate due to the support of elastic foundations. It is also observed from Table 8 that the critical dynamic buckling load increase sharply as the loading velocity  $s$  increases. This is due to the linear dependence of critical buckling load on the load velocity.

### 6.3. Frequency ratio – amplitude relation

The effect of width-to-thickness ratio  $b/h$  on the nonlinear to linear frequency ratio – amplitude relation of the smart sandwich plate is illustrated in Fig. 2. The geometrical parameters are taken to be  $a/b = 1$ ,  $h_c/h_f = 5$ ,  $h_c/h_p = 10$  while the temperature increment and applied voltage are taken to be  $\Delta T = 100\text{ K}$ ,  $V_p = 200\text{ V}$ . It can be clearly seen that the width-to-thickness ratio has considerable effect on the relation between frequency ratio and amplitude. With the same value of amplitude, the increase of the width-to-thickness ratio causes to the decrease of frequency ratio.

Fig. 3 investigates the effect of elastic foundations coefficients  $k_1$  (GPa/m) and  $k_2$  (GPa.m) on the frequency ratio – amplitude relation of the smart sandwich plate. Three cases of  $(k_1, k_2) = (0, 0)$ ,  $(0.3, 0)$ ,  $(0.3, 0.02)$  are considered. It can be observed that the frequency ratio decreases as two coefficients  $k_1$  and  $k_2$  increase with the same value of the amplitude due to the increase of the elastic modulus of the smart sandwich plate by the support of elastic foundations. Moreover, the effect of Pasternak foundation with modulus  $k_2$  is more pronounced than one of Winkler foundation with stiffness  $k_1$ .

Fig. 4 depicts the effect of the temperature increment  $\Delta T$  on the frequency ratio – amplitude relation of the smart sandwich plate. The CNT volume fraction is  $V_{CNT}^* = 0.12$  and the porosity coefficient is  $e_0 = 0.2$ . The results show that the frequency ratio with the same amplitude will become higher when the temperature increment increases. The physical explanation is that, the stiffness of the plate decreases under the impact of high temperature environment.

### 6.4. Nonlinear dynamic response

Fig. 5 demonstrates the effect of temperature increment  $\Delta T$  on the nonlinear dynamic response of the smart sandwich plate with simply supported edges subjected to uniform external pressure. The non-uniform symmetric is the porosity distribution type. The geometrical parameters are taken to be  $a/b = 1$ ,  $b/h = 20$ ,  $h_c/h_f = 5$ ,  $h_c/h_p = 10$ . It is evident that the temperature increment has the negative effect on the nonlinear dynamic response of the sandwich plate, an increase of the temperature increment leads to a rise of deflection amplitude. This is easy to explain because the increase of temperature causes the reduction in the stiffness of the sandwich plate.

Figs. 6 and 7 represent the relation between deflection amplitude of the smart sandwich plate with various values of modulus  $k_1$  and stiffness  $k_2$  of elastic foundations. Three values of  $k_1 = 0, 0.1\text{ GPa/m}, 0.3\text{ GPa/m}$  and three values of  $k_2 = 0, 0.02\text{ GPa.m}, 0.04\text{ GPa.m}$  are used. It is easy to see that the deflection amplitude of the sandwich plate decreases with the increase of elastic foundations coefficients  $k_1$  and  $k_2$ . This is because of the opposite impact of the elastic foundation compared to the direction of the applied loading. By comparing Figs. 6 and 7, it also can be found that the effect of Winkler foundation on buckling behaviors of the sandwich plate is greater than the Pasternak foundation. This is due to the nonlinear relationship between Pasternak foundation and deflection as well as the linear relationship between Winkler foundation and the deflection.

Fig. 8 shows the effect of CNT volume fraction  $V_{CNT}^*$  on the nonlinear dynamic response of the smart sandwich plate. The elastic foundation coefficients are taken to be  $k_1 = 0.3\text{ GPa/m}$ ,  $k_2 = 0.03\text{ GPa.m}$ , the temperature increment and applied voltage are chosen as  $\Delta T = 100\text{ K}$ ,  $V_p = 200\text{ V}$ . From Fig. 8, it is observed that the increase of CNT volume fraction results in the decrease of the deflection amplitude of the

sandwich plate. This is due to the enhancement in the stiffness of the sandwich plate by the reinforcement of CNT.

Fig. 9 presents the effect of porosity coefficient  $e_0$  on the nonlinear dynamic response of the smart sandwich plate with porous core layer in thermal environments. The dimensionless parameters are taken to be  $a/b = 1$ ,  $b/h = 20$ ,  $h_c/h_f = 5$ ,  $h_c/h_p = 10$ . The elastic foundations coefficients are  $k_1 = 0.3\text{ GPa/m}$ ,  $k_2 = 0.02\text{ GPa.m}$ . It is deduced from Fig. 9 that an increase of porosity coefficient leads to an increase of the deflection amplitude of the smart sandwich plate. It is easy to explain because the mass of the plate reduces as the porosity coefficient increases, which results in the reduction of the stiffness of the smart sandwich plate.

Fig. 10 expresses the nonlinear dynamic response of the smart sandwich plate for different values of initial imperfection amplitude ( $W_0 = 0, 0.005\text{ m}$  and  $0.01\text{ m}$ ). The CNT volume fraction is chosen as  $V_{CNT}^* = 0.12$  and the porosity coefficient is  $e_0 = 0.2$ . Obviously, the initial imperfection parameter has small effect on the nonlinear dynamic response of the smart sandwich plate. The higher initial imperfection amplitude is, the lower amplitude deflection is. This is due to the impact of initial imperfections, the total amplitude deflection of the smart sandwich plate changes from  $w$  to  $w + w^*$ .

The influence of the applied voltage  $V_p$  on the nonlinear dynamic response of smart the sandwich plate with  $a/b = 1$ ,  $b/h = 20$ ,  $h_c/h_f = 5$ ,  $h_c/h_p = 10$ ,  $W_0 = 0$ ,  $e_0 = 0.2$ ,  $V_{CNT}^* = 0.12$ ,  $\Delta T = 100\text{ K}$  is considered in Fig. 11. As can be seen, the applied voltage has small effect on the deflection amplitude of the smart sandwich plate. It can be found that the deflection amplitude increases slightly when the applied voltage increases. This is due to the reduction of the stiffness of the sandwich plate with the impact of applied voltage.

### 6.5. Optimum value of natural frequency

Bees Algorithm is conducted in 25 times and the optimum value of natural frequency of the smart sandwich plate is defined as the average value of 25 obtained values. In each time, the loop of stops if the number of objective function evaluation reaches to 40,000. Finally, the maximum value of the natural frequency is 70118.45 (1/s) when optimum values of nine variables are shown in Table 9.

Fig. 12 illustrates the convergence of the optimum value of the natural frequency according to the number of objective function evaluation in one loop of Bees Algorithm. As can be observed, the optimum value of the natural frequency rises sharply in the first numbers of objective function evaluation and then gradually reaches to the final value.

## 7. Concluding remarks

This paper introduces analytical solutions for the nonlinear vibration and critical dynamic buckling of an imperfect smart sandwich plate on elastic foundations based on Reddy' higher order shear deformation plate theory. The sandwich plate has five layers including one porous core, two CNTRC layers and two piezoelectric face sheets. The plate is subjected to the combination of mechanical, thermal and electric loadings. Various parameter studies are performed to consider the effect of geometrical and material parameters, elastic foundations and external impacts on the critical buckling load, nonlinear dynamic response and the frequency – amplitude relation of the smart sandwich plate. Bees Algorithm is used to determine the maximum value of the natural frequency. Major conclusions include:

- An increase of elastic foundations coefficients  $k_1$ ,  $k_2$  results in a decrease of the deflection amplitude and frequency ratio as well as a rise of critical dynamic buckling load of the smart sandwich plate. This is due to the enhancement of the stiffness of the plate by the support of elastic foundations.

- The porosity coefficient has negligible effect on the vibration and dynamic buckling of the sandwich plate. Although the deflection amplitude increases and the critical buckling load decreases as the porosity coefficient increases, the difference is acceptable. Further, the critical dynamic buckling load of the plate with uniform porosity distribution is higher than one with non-uniform porosity distribution.
- The addition of CNT increases the stiffness of the sandwich plate. Consequently, the deflection amplitude of the plate decreases when the CNT volume fraction increases. However, the critical dynamic buckling load of the plate becomes lower as the CNT volume fraction rises. Therefore, it is necessary to carefully consider the ratio of the CNT into the structure to ensure different technical requirements and usage goals.
- Temperature increment is considered as external impact. However, the effect of temperature increment on the mechanical behaviors of the sandwich plate is special as CNT volume fraction. The amplitude deflection and the frequency relation increase when the temperature increment increases. However, the critical dynamic buckling load also rises with the increase of temperature increment.
- The geometrical parameters  $b/h$  and  $a/b$  have significant effect on the critical dynamic buckling load and frequency ratio – amplitude relation of smart sandwich plate.

- As the initial imperfection amplitude rises, the deflection amplitude of the smart sandwich plate decreases slightly.
- The optimum value of natural frequency with constant geometrical and material parameters is 70118.45 (1/s).

**Author statement**

Authors could like to declare contributions to the manuscript: MSc. Ngo Dinh Dat: Formal analysis, Investigation, Writing - original, Dr. Tran Quoc Quan: Supervision, Methodology, Writing – review & editing. Prof. Nguyen Dinh Duc: Conceptualization, Data curation, Validation. There is no further information on the funding.

**Funding**

This research is funded by Vietnam National Foundation for Science and Technology Development (NAFOSTED) under grant number 107.02–2019.01. The authors are grateful for this support.

**Declaration of competing interest**

The authors declare no conflict of interest.

**Appendix A**

$$\begin{aligned}
 (A_{ij}, B_{ij}, D_{ij}, E_{ij}, F_{ij}, H_{ij}) &= \int_{-h_f-h_c/2-h_p}^{-h_c/2-h_f} Q_{ij}(1, z, z^2, z^3, z^4, z^6) dz + \int_{-h_f-h_c/2}^{-h_c/2} Q_{ij}(1, z, z^2, z^3, z^4, z^6) dz + \int_{-h_c/2}^{h_c/2} Q_{ij}(1, z, z^2, z^3, z^4, z^6) dz \\
 &+ \int_{h_c/2}^{h_c/2+h_f} Q_{ij}(1, z, z^2, z^3, z^4, z^6) dz + \int_{h_c/2+h_f}^{h_c/2+h_f+h_p} Q_{ij}(1, z, z^2, z^3, z^4, z^6) dz, \quad ij = 11, 12, 22, 66, \\
 (A_{kl}, D_{kl}, F_{kl}) &= \int_{-h_p-h_f-h_c/2}^{-h_f-h_c/2} Q_{ij}(1, z^2, z^4) dz + \int_{-h_f-h_c/2}^{-h_c/2} Q_{ij}(1, z^2, z^4) dz + \int_{-h_c/2}^{h_c/2} Q_{ij}(1, z^2, z^4) dz + \int_{h_c/2}^{h_c/2+h_f} Q_{ij}(1, z^2, z^4) dz + \int_{h_c/2+h_f}^{h_c/2+h_f+h_p} Q_{ij}(1, z^2, z^4) dz, \quad kl \\
 &= 44, 55, \\
 (\Phi_1, \Phi_3, \Phi_5) &= \int_{-h_f-h_c/2-h_p}^{-h_c/2-h_f} (Q_{11}^p \alpha_{11} \Delta T + Q_{12}^p \alpha_{22} \Delta T)(1, z, z^2) dz + \int_{-h_f-h_c/2}^{-h_c/2} (Q_{11}^f \alpha_{11} \Delta T + Q_{12}^f \alpha_{22} \Delta T)(1, z, z^2) dz + \int_{-h_c/2}^{h_c/2} (Q_{11}^c \alpha_{11} \Delta T + Q_{12}^c \alpha_{22} \Delta T)(1, z, z^2) dz \\
 &+ \int_{h_c/2}^{h_f+h_c/2} (Q_{11}^f \alpha_{11} \Delta T + Q_{12}^f \alpha_{22} \Delta T)(1, z, z^2) dz + \int_{h_c/2+h_f}^{h_f+h_c/2+h_p} (Q_{11}^p \alpha_{11} \Delta T + Q_{12}^p \alpha_{22} \Delta T)(1, z, z^2) dz + \int_{h_c/2}^{h_f+h_c/2} (Q_{12}^f \alpha_{11} \Delta T + Q_{22}^f \alpha_{22} \Delta T)(1, z, z^2) dz \\
 &+ \int_{h_c/2+h_f}^{h_f+h_c/2+h_p} (Q_{12}^p \alpha_{11} \Delta T + Q_{22}^p \alpha_{22} \Delta T)(1, z, z^2) dz, \quad (\Phi_2, \Phi_4, \Phi_6) \\
 &= \int_{-h_f-h_c/2-h_p}^{-h_c/2-h_f} (Q_{12}^p \alpha_{11} \Delta T + Q_{22}^p \alpha_{22} \Delta T)(1, z, z^2) dz + \int_{-h_f-h_c/2}^{-h_c/2} (Q_{12}^f \alpha_{11} \Delta T + Q_{22}^f \alpha_{22} \Delta T)(1, z, z^2) dz + \int_{-h_c/2}^{h_c/2} (Q_{12}^c \alpha_{11} \Delta T + Q_{22}^c \alpha_{22} \Delta T)(1, z, z^2) dz \\
 &+ \int_{h_c/2}^{h_f+h_c/2} (Q_{12}^f \alpha_{11} \Delta T + Q_{22}^f \alpha_{22} \Delta T)(1, z, z^2) dz + \int_{h_c/2+h_f}^{h_f+h_c/2+h_p} (Q_{12}^p \alpha_{11} \Delta T + Q_{22}^p \alpha_{22} \Delta T)(1, z, z^2) dz,
 \end{aligned}$$

**Appendix B**

$$\begin{aligned}
 O_{11} &= A_{44} - 6c_1D_{44} + 9c_1^2F_{44}, \quad O_{12} = A_{55} - 6c_1D_{55} + 9c_1^2F_{55}, \quad O_{13} = -c_1^2(E_{11}I_{15} + E_{12}I_{25} + H_{11}), \\
 O_{14} &= -c_1^2(4E_{66}I_{33} + 4H_{66} + E_{11}I_{16} + E_{12}I_{26} + 2H_{12} + E_{12}I_{15} + E_{22}I_{25}), \\
 O_{15} &= -c_1^2(E_{12}I_{16} + E_{22}I_{26} + H_{22}), \quad O_{16} = c_1(E_{11}I_{13} - c_1E_{11}I_{15} + F_{11} - c_1H_{11} + E_{12}I_{23} - c_1E_{12}I_{25}), \\
 O_{17} &= c_1(2E_{66}I_{32} - 2c_1E_{66}I_{33} + 2F_{66} - 2c_1H_{66} + c_1E_{12}I_{13} - c_1E_{12}I_{15} + F_{12} - c_1H_{12} + E_{22}I_{23} - c_1E_{22}I_{25}), \\
 O_{18} &= c_1(E_{12}I_{14} - c_1E_{12}I_{16} + E_{22}I_{24} - c_1E_{22}I_{26} + F_{22} - c_1H_{22}), \quad O_{19} \\
 &= c_1(2E_{66}I_{32} - 2c_1E_{66}I_{33} + 2F_{66} - 2c_1H_{66} + E_{11}I_{14} - c_1E_{11}I_{16} + E_{12}I_{24} - c_1E_{12}I_{26} + F_{12} - c_1H_{12}), \quad O_{110} = -c_1(E_{11}I_{12} - E_{12}I_{21}), \quad O_{111} \\
 &= -c_1(2E_{66}I_{31} - E_{11}I_{11} + 2E_{12}I_{12} - E_{22}I_{21}), \quad O_{112} = c_1(E_{12}I_{11} - E_{22}I_{12}), \quad O_{21} = -A_{44} + 6c_1D_{44} - 9c_1^2F_{44}, \quad O_{22} \\
 &= -c_1(B_{11}I_{15} + F_{11} + B_{12}I_{25} - c_1E_{11}I_{15} - c_1H_{11} - c_1E_{12}I_{25}), \quad O_{23} \\
 &= -c_1(B_{11}I_{16} + B_{12}I_{26} + F_{12} + 2B_{66}I_{33} + 2F_{66} - 2c_1E_{66}I_{33} - 2c_1H_{66} - c_1E_{11}I_{16} - c_1E_{12}I_{26} - c_1H_{12}), \quad O_{24} \\
 &= B_{11}I_{13} - c_1B_{11}I_{15} + D_{11} - c_1F_{11} + B_{12}I_{23} - c_1B_{12}I_{25} - c_1E_{11}I_{13} + c_1^2E_{11}I_{15} - c_1F_{11} + c_1^2H_{11} - c_1E_{12}I_{23} + c_1^2E_{12}I_{25}, \quad O_{25} \\
 &= B_{66}I_{32} - c_1B_{66}I_{33} + D_{66} - c_1F_{66} - c_1E_{66}I_{32} + c_1^2E_{66}I_{33} - c_1F_{66} + c_1^2H_{66}, \quad O_{26} \\
 &= B_{11}I_{14} - c_1B_{11}I_{16} + B_{12}I_{24} - c_1B_{12}I_{26} + D_{12} - c_1F_{12} + B_{66}I_{32} - c_1B_{66}I_{33} + D_{66} - c_1F_{66} - c_1E_{66}I_{32} + c_1^2E_{66}I_{33} - c_1F_{66} + c_1^2H_{66} - c_1E_{11}I_{14} \\
 &\quad + c_1^2E_{11}I_{16} - c_1E_{12}I_{24} + c_1^2E_{12}I_{26} - c_1F_{12} \\
 &\quad + c_1^2H_{12}, \quad O_{27} = -B_{11}I_{12} + B_{12}I_{21} + c_1E_{11}I_{12} - c_1E_{12}I_{21}, \quad O_{28} = B_{11}I_{11} - B_{12}I_{12} - B_{66}I_{31} - c_1E_{11}I_{11} + c_1E_{12}I_{12} \\
 &\quad + c_1E_{66}I_{31}, \quad O_{31} = -A_{55} + 6c_1D_{55} - 9c_1^2F_{55}, \quad O_{32} = -c_1(2B_{66}I_{33} + 2F_{66} + B_{12}I_{15} + F_{12} + B_{22}I_{25} \\
 &\quad - 2c_1E_{66}I_{33} - 2c_1H_{66} - c_1E_{12}I_{15} - c_1H_{12} - c_1E_{22}I_{25}), \quad O_{33} = -c_1(B_{12}I_{16} + B_{22}I_{26} + F_{22} - c_1E_{12}I_{16} \\
 &\quad - c_1E_{22}I_{26} - c_1H_{22}), \quad O_{34} = B_{66}I_{32} - c_1B_{66}I_{33} + D_{66} - c_1F_{66} + B_{12}I_{13} - c_1B_{12}I_{15} + D_{12} - c_1F_{12} + B_{22}I_{23} \\
 &\quad - c_1B_{22}I_{25} - c_1E_{66}I_{32} + c_1^2E_{66}I_{33} - c_1F_{66} + c_1^2H_{66} - c_1E_{12}I_{13} + c_1^2E_{12}I_{15} - c_1F_{12} + c_1^2H_{12} - c_1E_{22}I_{23} \\
 &\quad + c_1^2E_{22}I_{25}, \quad O_{35} = B_{66}I_{32} - c_1B_{66}I_{33} + D_{66} - c_1F_{66} - c_1E_{66}I_{32} + c_1^2E_{66}I_{33} - c_1F_{66} + c_1^2H_{66}, \\
 O_{36} &= B_{12}I_{14} - c_1B_{12}I_{16} + B_{22}I_{24} - c_1B_{22}I_{26} + D_{22} - c_1F_{22} - c_1E_{12}I_{14} + c_1^2E_{12}I_{16} - c_1E_{22}I_{24} + c_1^2E_{22}I_{26} \\
 &\quad - c_1F_{22} + c_1^2H_{22}, \quad O_{37} = -B_{66}I_{31} - B_{12}I_{12} + B_{22}I_{21} + c_1E_{66}I_{31} + c_1E_{12}I_{12} - c_1E_{22}I_{21}, \\
 O_{38} &= B_{12}I_{11} - B_{22}I_{12} - c_1E_{12}I_{11} + c_1E_{22}I_{12}.
 \end{aligned}$$

**Appendix C**

$$\begin{aligned}
 l_{11} &= -k_1 - k_2(\lambda_m^2 + \delta_n^2) + X_{13}\lambda_m^4 + X_{14}\lambda_m^2\delta_n^2 + X_{15}\delta_n^4 + X_{110}Q_1\lambda_m^4 + X_{111}Q_1\lambda_m^2\delta_n^2 + X_{112}Q_1\delta_n^4, \\
 l_{12} &= -X_{11}\lambda_m + X_{16}\lambda_m^3 + X_{17}\lambda_m\delta_n^2 + X_{110}Q_2\lambda_m^4 + X_{111}Q_2\lambda_m^2\delta_n^2 + X_{112}Q_2\delta_n^4, \\
 l_{13} &= -X_{12}\delta_n + X_{18}\delta_n^3 + X_{19}\lambda_m^2\delta_n + X_{110}Q_3\lambda_m^4 + X_{111}Q_3\lambda_m^2\delta_n^2 + X_{112}Q_3\delta_n^4, \\
 l_{14} &= \frac{32Q_2\lambda_m\delta_n}{3ab}, \quad l_{15} = \frac{32Q_3\lambda_m\delta_n}{3ab}, \quad n_1 = -X_{11}\lambda_m^2 - X_{12}\delta_n^2, \quad n_2 = \frac{32Q_1\lambda_m\delta_n}{3ab}, \\
 n_3 &= -\frac{8X_{110}\lambda_m\delta_n}{3abl_{21}} - \frac{8X_{112}\lambda_m\delta_n}{3abl_{11}}, \quad n_4 = -\frac{\lambda_m^4}{16l_{11}} - \frac{\delta_n^4}{16l_{21}}, \quad n_5 = \frac{16}{mn\pi^2}, \\
 l_{21} &= -\lambda_m^3(X_{22} + Q_1X_{27}) - \lambda_m\delta_n^2(X_{23} + Q_1X_{28}), \quad l_{22} = X_{21} - X_{24}\lambda_m^2 - X_{25}\delta_n^2 - X_{27}Q_2\lambda_m^3 - X_{28}Q_2\lambda_m\delta_n^2, \\
 l_{23} &= -X_{26}\lambda_m\delta_n - X_{27}Q_3\lambda_m^3 - X_{28}Q_3\lambda_m\delta_n^2, \quad n_6 = X_{21}\lambda_m, \quad n_7 = \frac{8X_{27}\delta_n}{3abl_{21}}, \quad l_{31} = -\delta_n^3(X_{33} + Q_1X_{38}) \\
 &\quad - \lambda_m^2\delta_n(X_{32} + Q_1X_{37}), \quad l_{32} = -X_{34}\lambda_m\delta_n - X_{38}Q_2\delta_n^3 - D_{37}Q_2\lambda_m^2\delta_n, \quad l_{33} = X_{31} - X_{35}\lambda_m^2 - X_{36}\delta_n^2 \\
 &\quad - X_{38}Q_3\delta_n^3 - X_{37}Q_3\lambda_m^2\delta_n, \quad n_8 = X_{31}\delta_n, \quad n_9 = \frac{8X_{38}\lambda_m}{3abl_{11}}.
 \end{aligned}$$

**Appendix D**

$$\begin{aligned}
 \bar{J}_0 &= J_0 - (l_{12}a_{14} + l_{13}a_{24}), \quad J_0^* = (l_{14}^1a_{14} + l_{15}^1a_{24}), \quad a_{11} = -\frac{(l_{21}l_{33} - l_{23}l_{31})}{(l_{22}l_{33} - l_{23}l_{32})}, \quad a_{12} = -\frac{(n_6l_{33} - n_8l_{23})}{(l_{22}l_{33} - l_{23}l_{32})}, \quad a_{13} = -\frac{(n_7l_{33} - n_9l_{23})}{(l_{22}l_{33} - l_{23}l_{32})}, \quad a_{14} = \left( -\lambda_m \bar{J}_5 l_{33} + \delta_n \bar{J}_5 l_{23} \right) \\
 (l_{22}l_{33} - l_{23}l_{32}), \quad s_{11} &= (l_{11}^1 + l_{12}a_{11} + l_{13}a_{21}), \quad s_{12} = (n_1^1 + l_{12}a_{12} + l_{13}a_{22}), \quad s_{13} = (n_2^1 + l_{14}^1a_{11} + l_{15}^1a_{21}), \quad s_{14} = (n_3 + l_{12}a_{13} + l_{13}a_{23}), \quad s_{15} = (l_{14}^1a_{12} + l_{15}^1a_{22}), \quad s_{16} = (n_4^1 + l_{14}^1a_{13} + l_{15}^1a_{23}).
 \end{aligned}$$

## References

- Alibeigloo, A., 2019. Coupled thermoelasticity analysis of FGM plate integrated with piezoelectric layers under thermal shock. *J. Therm. Stresses* 42, 1357–1375. <https://doi.org/10.1080/01495739.2019.1640653>.
- Ansari, R., Hassani, R., Gholami, R., Rouhi, H., 2020. Nonlinear bending analysis of arbitrary-shaped porous nanocomposite plates using a novel numerical approach. *Int. J. Non Lin. Mech.* 126, 103556. <https://doi.org/10.1016/j.jnlinmec.2020.103556>.
- Babaei, H., Eslami, M.R., Khorshidvand, A.R., 2020. Thermal buckling and postbuckling responses of geometrically imperfect FG porous beams based on physical neutral plane. *J. Therm. Stresses* 43, 109–131. <https://doi.org/10.1080/01495739.2019.1660600>.
- Bush, D.D., Almroth, B.O., 1975. *Buckling of Bars, Plates and Shells*. Mc Graw-Hill.
- Budiansky, B., Roth, R.S., 1962. Axisymmetric dynamic buckling of clamped shallow spherical shells. *NASA Tech. Note D 510*, 597–609.
- Chen, H., Ma, J., Liu, H., 2018. Least square spectral collocation method for nonlinear heat transfer in moving porous plate with convective and radiative boundary conditions. *Int. J. Therm. Sci.* 132, 335–343. <https://doi.org/10.1016/j.ijthermalsci.2018.06.020>.
- Chen, D., Yang, J., Kitipornchai, S., 2019. Buckling and bending analyses of a novel functionally graded porous plate using Chebyshev-Ritz method. *Arch. Civ. Mech. Eng.* 19, 157–170. <https://doi.org/10.1016/j.acme.2018.09.004>.
- Dat, N.D., Quan, T.Q., Mahesh, V., Duc, N.D., 2020. Analytical solutions for nonlinear magneto-electro-elastic vibration of smart sandwich plate with carbon nanotube reinforced nanocomposite core in hygrothermal environment. *Int. J. Mech. Sci.* 186, 105906. <https://doi.org/10.1016/j.ijmecsci.2020.105906>.
- Duc, N.D., Hadavinia, H., Quan, T.Q., Khoa, N.D., 2019. Free vibration and nonlinear dynamic response of imperfect nanocomposite FG-CNTRC double curved shallow shells in thermal environment. *Eur. J. Mech. Solid.* 75, 355–366. <https://doi.org/10.1016/j.euromechsol.2019.01.024>.
- Farsangi, M.A.A., Saidi, A.R., Batra, R.C., 2013. Analytical solution for free vibrations of moderately thick hybrid piezoelectric laminated plates. *J. Sound Vib.* 332, 5981–5998. <https://doi.org/10.1016/j.jsv.2013.05.010>.
- Fu, T., Wu, X., Xiao, Z., Chen, Z., 2021. Dynamic instability analysis of FG-CNTRC laminated conical shells surrounded by elastic foundations within FSDT. *Eur. J. Mech. Solid.* 85, 104139. <https://doi.org/10.1016/j.euromechsol.2020.104139>.
- Giannopoulos, G., Santafe, F., Monreal, J., Vantomme, J., 2007. Thermal, electrical, mechanical coupled mechanics for initial buckling analysis of smart plates and beams using discrete layer kinematics. *Int. J. Solid Struct.* 44, 4707–4722. <https://doi.org/10.1016/j.ijsolstr.2006.11.048>.
- Karimiasl, M., Ebrahimi, F., Mahesh, V., 2019. Nonlinear forced vibration of smart multiscale sandwich composite doubly curved porous shell. *Thin-Walled Struct.* 143, 106152. <https://doi.org/10.1016/j.tws.2019.04.044>.
- Mahmoodi, M.J., Rajabi, Y., Khodaiepour, B., 2020. Electro-thermo-mechanical responses of laminated smart nanocomposite moderately thick plates containing carbon nanotube-A multi-scale modeling. *Mech. Mater.* 141, 103247. <https://doi.org/10.1016/j.mechmat.2019.103247>.
- Moradi-Dastjerdi, R., Behdinin, K., Safaei, B., Qin, Z., 2020. Buckling behavior of porous CNT-reinforced plates integrated between active piezoelectric layers. *Eng. Struct.* 222, 111141. <https://doi.org/10.1016/j.engstruct.2020.111141>.
- Pham, D.T., Castellani, M., 2009. The Bees Algorithm: modelling foraging behavior to solve continuous optimization problems. *Proc. Inst. Mech. Eng. Part C J. Mech. Eng. Sci.* 223, 2919–2938. <https://doi.org/10.1243/09544062JMES1494>.
- Qin, B., Zhong, R., Wang, T., Wang, Q., Xu, Y., Hu, Z., 2020. A unified Fourier series solution for vibration analysis of FG-CNTRC cylindrical, conical shells and annular plates with arbitrary boundary conditions. *Compos. Struct.* 232, 111549. <https://doi.org/10.1016/j.compstruct.2019.111549>.
- Reddy, J.N., 2004. *Mechanics of Laminated Composite Plates and Shells: Theory and Analysis*. CRC Press, Boca Raton.
- Sahoo, S.R., Ray, M.C., 2019. Active damping of geometrically nonlinear vibrations of smart composite plates using elliptical SCLD treatment with fractional derivative viscoelastic layer. *Eur. J. Mech. Solid.* 78, 103823. <https://doi.org/10.1016/j.euromechsol.2019.103823>.
- Saidi, A.R., Bahaadini, R., Majidi-Mozafari, K., 2019. On vibration and stability analysis of porous plates reinforced by graphene platelets under aerodynamical loading. *Compos. B Eng.* 164, 778–799. <https://doi.org/10.1016/j.compositesb.2019.01.074>.
- Shankar, G., Keshava Kumar, S., Mahato, P.K., 2017. Vibration analysis and control of smart composite plates with delamination and under hygrothermal environment. *Thin-Walled Struct.* 116, 53–68. <https://doi.org/10.1016/j.tws.2017.03.013>.
- Shen, H.S., Wang, H., 2017. Nonlinear vibration of compressed and thermally postbuckled nanotube-reinforced composite plates resting on elastic foundations. *Aero. Sci. Technol.* 64, 63–74. <https://doi.org/10.1016/j.ast.2017.01.017>.
- Shen, H.S., Wang, H., Yang, D.Q., 2017. Vibration of thermally postbuckled sandwich plates with nanotube-reinforced composite face sheets resting on elastic foundations. *Int. J. Mech. Sci.* 124 (125), 253–262. <https://doi.org/10.1016/j.ijmecsci.2017.03.015>.
- Shen, H.S., Xiang, Y., 2013. Nonlinear analysis of nanotube-reinforced composite beams resting on elastic foundations in thermal environments. *Eng. Struct.* 56, 698–708. <https://doi.org/10.1016/j.engstruct.2013.06.002>.
- Shen, H.S., Xiang, Y., 2014. Nonlinear vibration of nanotube-reinforced composite cylindrical panels resting on elastic foundations in thermal environments. *Compos. Struct.* 111, 291–300. <https://doi.org/10.1016/j.compstruct.2014.01.010>.
- Sofiyev, A.H., Turkaslan, B.E., Bayramov, R.P., Salamci, M.U., 2019. Analytical solution of stability of FG-CNTRC conical shells under external pressures. *Thin-Walled Struct.* 144, 106338. <https://doi.org/10.1016/j.tws.2019.106338>.
- Sofiyev, A.H., 2020. On the vibration and stability behaviors of heterogeneous-CNTRC-truncated conical shells under axial load in the context of FSDT. *Thin-Walled Struct.* 151, 106747. <https://doi.org/10.1016/j.tws.2020.106747>.
- Sreehari, V.M., George, L.J., Maiti, D.K., 2016. Bending and buckling analysis of smart composite plates with and without internal flaw using an inverse hyperbolic shear deformation theory. *Compos. Struct.* 138, 64–74. <https://doi.org/10.1016/j.compstruct.2015.11.045>.
- Srinivas, S., Joga Rao, C.V., Rao, A.K., 1970. An exact analysis for vibration of simply supported homogeneous and laminate thick rectangular plates. *J. Sound Vib.* 12, 187–199. [https://doi.org/10.1016/0022-460X\(70\)90089-1](https://doi.org/10.1016/0022-460X(70)90089-1).
- Trinh, M.C., Mukhopadhyay, T., Kim, S.E., 2020. A semi-analytical stochastic buckling quantification of porous functionally graded plates. *Aero. Sci. Technol.* 105, 105928. <https://doi.org/10.1016/j.ast.2020.105928>.
- Xie, K., Wang, Y., Niu, H., Chen, H., 2020. Large-amplitude nonlinear free vibrations of functionally graded plates with porous imperfection: a novel approach based on energy balance method. *Compos. Struct.* 246, 112367. <https://doi.org/10.1016/j.compstruct.2020.112367>.
- Xue, Y., Jin, G., Ma, X., Chen, H., Ye, T., Chen, M., Zhang, Y., 2019. Free vibration analysis of porous plates with porosity distributions in the thickness and in-plane directions using isogeometric approach. *Int. J. Mech. Sci.* 152, 346–362. <https://doi.org/10.1016/j.ijmecsci.2019.01.004>.
- Yang, J., Huang, X.H., Shen, H.S., 2020. Nonlinear vibration of temperature-dependent FG-CNTRC laminated plates with negative Poisson's ratio. *Thin-Walled Struct.* 148, 106514. <https://doi.org/10.1016/j.tws.2019.106514>.
- Zhang, L.W., Pan, Z.Z., Chen, X., 2020. Vibration characteristics of matrix cracked pretwisted hybrid composite blades containing CNTRC layers. *J. Sound Vib.* 473, 115242. <https://doi.org/10.1016/j.jsv.2020.115242>.
- Zhu, P., Lei, Z.X., Liew, K.M., 2012. Static and free vibration analyses of carbon nanotube-reinforced composite plates using finite element method with first order shear deformation plate theory. *Compos. Struct.* 94, 1450–1460. <https://doi.org/10.1016/j.compstruct.2011.11.010>.
- Zoric, N.D., Tomovic, A.M., Obradovic, A.M., Radulovic, R.D., Petrovic, G.R., 2019. Active vibration control of smart composite plates using optimized self-tuning fuzzy logic controller with optimization of placement, sizing and orientation of PFR actuators. *J. Sound Vib.* 456, 173–198. <https://doi.org/10.1016/j.jsv.2019.05.035>.